The distribution of particulate organic matter in the heterogeneous soil matrix - balancing between aerobic respiration and denitrification.

Maik Lucas [1,2,*], Lena Rohe [3], Bernd Apelt [1], Claus Florian Stange [4], Hans-Jörg Vogel [1] , Reinhard Well [3] and Steffen Schlüter [1]

[1] *Helmholtz Centre for Environmental Research - UFZ, Department Soil System Sciences, Halle (Saale), Germany*
[2] *Institute of Ecology, Chair of Soil Science, Technical University Berlin, 10587 Berlin, Germany*
[3] *Thünen Institute of Climate-Smart Agriculture, Bundesallee 65, 38116 Braunschweig, Germany*
[4] *Federal Institute for Geoscience and Natural Resources-BGR, Department Soil as Resource - Properties and Dynamics, Stilleweg 2, 30655 Hannover, Germany*

Correspondence*:
Corresponding Author
ml@boku.tu-berlin.de

ABSTRACT

Denitrification, a key process in soil nitrogen cycling, occurs predominantly within microbial hotspots, where denitrifiers use nitrate as an alternative electron acceptor. For accurate prediction of dinitrogen (N2) and nitrous oxide (N_2O) emissions from denitrification, a precise quantification of these microscale hotspots is required.

Employing a unique combination of X-ray CT imaging, microscale O_2 measurements, and ^{15}N labeling, we were able to quantify hotspots of aerobic respiration and denitrification. We analyzed the dynamics of greenhouse gas (GHG) fluxes, soil oxygen supply, and the distribution of particulate organic matter (POM) in intact soil samples from a grassland and a cropland under different moisture conditions. Our findings reveal that both free and occluded particulate organic matter (POM), identified through X-ray CT imaging, contribute to GHG emissions. The occluded POM, i.e. POM at distant locations to air-filled pores, emerged as a primary driver of denitrification within structured soils of both land uses. Thus, the higher denitrification rates in the grassland could be attributed to the higher content of occluded POM. Conversely, despite possessing compacted areas that could favor denitrification, the cropland had only small amounts of occluded POM to stimulate denitrification. This underlines the complex interaction between soil structural heterogeneity, organic carbon supply, and microbial hotspot formation and thus contributes to a better understanding of soil-related GHG emissions.

In summary, our study provides a holistic understanding of soil-borne greenhouse gas emissions and emphasizes the need to refine predictive models for soil denitrification and N_2O emissions by incorporating the microscale distribution of POM.

Keywords: nitrous oxide, soil structure, X-ray CT, greenhouse gases, carbon dioxide

1 INTRODUCTION

Nitrous oxide (N_2O) and dinitrogen (N_2) emissions from soil significantly impair the nitrogen (N) use efficiency of crops and contribute to global climate change due to the potent greenhouse effect of N_2O and its role in stratospheric ozone depletion (Ravishankara et al. 2009; Tian et al. 2020). Microbial processes, particularly denitrification, play a pivotal role in N_2O production, exhibiting complex dependencies on soil structure, moisture, and organic matter content. These dependencies are further complicated by microscale heterogeneity within soils, with completely different microenvironmental conditions at short spatial scales such as oxygen (O_2) availability or the presence and absence of easily degradable carbon sources. O_2 availability at the microscale determines the occurrence of either aerobic respiration or anaerobic respiration like denitrification. The latter reduces nitrate (NO_3-) to nitrogen gas (N_2), with nitrous oxide (N_2O) as an intermediate (Firestone et al. 1989; Philippot et al. 2007; G P Robertson 2023). In contrast, aerobic conditions lead to organic carbon mineralization rates and consequent carbon dioxide (CO_2) release approximately ten times higher than those under anaerobic conditions due to the higher energy yield of aerobic respiration (Keiluweit, Wanzek, et al. 2017; Lacroix, Aeppli, et al. 2023). At locations known as hotspots, such as the detritusphere of plant residues, increased C availability leads to intensive microbial activity and thus to increased process rates (Groffman et al. 2009; Kuzyakov et al. 2015). While, however, the presence of microbial hotspots and their heterogeneous distribution in soil are generally recognized (Kuzyakov et al. 2015; Lacroix, Aeppli, et al. 2023), their quantification remains a challenge.

Yet, a significant advancement in understanding denitrification hotspots, comes from examining the spatial distribution of carbon sources and the O_2 depletion related to its decomposition. Illustratively, Parkin 1987 found that nearly all denitrification within a soil core could be traced back to a decomposing plant leaf. The persistence and activity of denitrifying enzymes in overall well-aerated soils were therefore attributed to these potential microsites of anaerobiosis around decomposing particulate organic matter (POM, Surey et al. 2020), indicating the nuanced interplay of environmental factors in soils. POM particles, hotspots of oxygen consumption, are distributed non-randomly within the soil matrix (Højberg et al. 1994; Kravchenko and Guber 2017; Parkin 1987; Schlüter, Leuther, et al. 2022). One reason for this non-random distribution is that a large share of POM originates from roots which predominately grow into more loose areas or directly into macropores (Lucas, Nguyen, et al. 2022; Lucas, Schlüter, et al. 2019a; White et al. 2010). The distribution of POM is further modulated by land use (John et al. 2005). While tillage practices on croplands lead to a vertical mixing of crop residues with soil it also reduces the amount of soil fauna like anecic earthworms, which were shown to incorporate POM into the soil matrix (Briones et al. 2017; Leuther et al. 2023; Wilkinson et al. 2009; Yang et al. 1999). On perennial grassland, permanently covered by vegetation, bioturbation rates and thus incorporation of POM into the soil matrix are higher compared to tilled croplands (Kraus et al. 2022; Stolze et al. 2022).

Oxygen availability at the microscale results from a delicate balance between oxygen consumption through microbial respiration, and supply via diffusion (Keiluweit, Nico, et al. 2016). In contrast to the distribution of POM, which controls the local O_2 demand, it is the configuration of the air-filled pore space that determines the diffusion distances of dissolved oxygen through the wet soil matrix (Du et al. 2023; Rohe et al. 2021). This pore space is influenced by processes such as bioturbation (Lucas, Schlüter, et al. 2019b; Wilkinson et al. 2009), wetting-drying cycles (Diel et al. 2019; Fomin et al. 2023), or tillage practices (Pires et al. 2017; Schlüter, Großmann, et al. 2018; Wardak et al. 2022). As a consequence, both, diffusion distances of dissolved O_2 through the soil matrix, i.e. O_2 supply (Lucas, Santiago, et al. 2023; Schlüter, Leuther, et al. 2022), and the local O_2 demand depend on the type of land use and with it underlying redox reactions (Lacroix, Aeppli, et al. 2023).

Historically, the quantification of anaerobic soil volume fraction and its role in denitrification has been limited by the resolution of available measurement techniques. Recent technological advances, such as X-ray computed tomography (CT) imaging and microscale oxygen measurements, have begun to unveil the complex interplay between soil structure, oxygen dynamics, and microbial hotspots of activity. X-ray microtomography has been applied repeatedly to determine the volume fraction and distribution of air-filled pores to help predict N_2O emissions (Kravchenko, Guber, et al. 2018; Lucas, Santiago, et al. 2023; Rabot et al. 2015; Rohe et al. 2021). Most recently two of these studies revealed that enhanced N_2O emissions are caused by larger volumes of POM at greater distances to pores, here denoted as occluded POM (Lucas, Santiago, et al. 2023; Ortega-Ramírez et al. 2023). In contrast, larger amounts of POM located within or close to pores should result in large CO_2 emissions from aerobic respiration.

Our study aims to provide a comprehensive understanding of how microscale heterogeneities, specifically the distribution of POM relative to pore structure, influence N_2, N_2O and CO_2 emissions in structured soils. We evaluate results from an incubation experiment with undisturbed soil cores from contrasting environments (cropland vs. grassland) under varying water contents. The combination of X-ray CT imaging with microsensors and ^{15}N labeling was used for a nuanced exploration of the interplay between soil structure, moisture, and microbial activity, and their collective impact on CO_2 and N_2O+N_2 fluxes. Furthermore, we compare our findings with a previous study using sieved soil without large POM fragments originating from the same sites to understand better the impacts of soil architecture and POM on denitrification processes.

2 METHODS

2.1 Soil sampling and preparation

In June 2022 undisturbed cores were collected from two sites in Germany representing two land uses. The first land use was situated in Rotthalmünster at latitude N48°21', longitude E13°11' and had a Haplic Luvisol with a silty loam texture and a pH of 7.21, originated from an arable field in Rotthalmünster. This field, which undergoes regular plowing to a depth of 30 cm, is subsequently referred to as 'cropland'. The second land use was an extensively managed grassland in Gießen, hereafter named 'grassland', located at latitude N50°32', longitude E8°41'. The soil was a Fluvic Gleysol with a clay loam texture, containing 4.42% soil organic carbon (SOC) and a pH of 6.71, exhibiting a higher soil organic matter (SOM) content of 4.46% and a lower bulk density of 1.0 g cm^{-3} compared to the 'cropland' soil, which had SOC contents of 1.21% and a bulk density of 1.3 g cm^{-3}, as detailed in Rohe et al. 2021. For sampling, a specialized drill (UGT GmbH, Germany) for the undisturbed collection of cylindrical soil cores, was employed. These samples, encased in rigid 5 mm PE sleeves, consisted of five undisturbed cores per land use, each measuring 10 cm in height and diameter, extracted from a soil depth of 5-15 cm. The samples were air-dried until a moisture content of pF=3 was reached and stored at 4°C until further processing. At the 'cropland', wheat had been harvested just before sampling. Our incubation setup follows the line of Rohe et al. 2021 which we refer to for more information on the field sites. In the referenced study, soils were sieved to remove particulate organic matter (POM) to isolate the effects of pore distances on denitrification. Here, we employ the same soil and incubation setup, but with intact field-structured soil, to investigate how POM affects oxygen distribution and thereby influences hotspots of denitrification. A solution containing ^{15}N was created by combining $^{15}NKNO_3$ with a 99 atomic percent (^{15}N) purity (Cambridge Isotope Laboratories, Inc., Andover, MA, USA) and unlabelled KNO_3 (Merck, Darmstadt, Germany). The objective was to achieve a nitrogen concentration of 50 mg N kg^{-1} of soil, with the ^{15}N-labelled KNO_3 making up 60 atomic percent of the nitrogen in each level of water saturation treatment. Consequently, appropriate dilution of the stock solution was applied to ensure the same nitrate concentration and isotopic enrichment in treatments

with different soil moisture. We developed a setup, which assured an even distribution of the ^{15}N-KNO_3 label within the structured cores. In short, we saturated the samples from below with the NO_3 solution overnight, then irrigated the samples from above with fresh ^{15}N-KNO_3 solution at a flow corresponding to the saturated conductivity until three times the pore volume of a cylinder was flushed through the sample. After this, we adjusted the moisture content of the cores by connecting a hanging water column of -160 cm, -40 cm, and -8 cm to the bottom of the cores corresponding roughly to a water-holding capacity of 95%, 80%, and 70%. The labeling procedure took place in a 7°C fridge. For the two-factorial study design with two land uses, three moisture contents, and three replicates we incubated nine undisturbed cores per land use.

2.2 Incubation

The columns were closed tightly and equipped with an inlet and outlet in the headspace (Fig. 1). Seven holes were drilled radially in the center of the column to install oxygen microsensors (40×0.8 mm) with <140 μm flatbroken sensor tips (NFSG-PSt1, PreSens Precision Sensing GmbH, Regensburg, Germany). The microsensors were attached to a multi-channel oxygen meter (OXY-10 micro, PreSens Precision Sensing GmbH, Regensburg, Germany) to log O_2 concentration in 30-minute intervals. During the incubation, the columns were placed in a temperature-controlled (20°C) bath and darkened water bath (JULABO GmbH, Seelbach, Germany). A constant flow of a helium gas containing 21% O_2 and 0.5% N_2 (5 ml min^{-1}) was set throughout the 250 h incubation ($\backsim$ 11 days) using flow controllers (G040, Brooks® Instrument, Dresden, Germany). This atmosphere with low- N_2 concentration was used to increase the sensitivity for N_2 fluxes (Lewicka-Szczebak et al. 2017). Before incubation started, the headspace was flushed with technical gas for approx. three hours under three cycles of light vacuum (max. 300 mbar) to reduce the N_2 concentration in the soil column to approximately that of the technical gas and to ensure comparable initial conditions for the incubation. Our setup allowed the incubation of a block of three parallel samples, i.e. with all three moisture contents simultaneously.

2.3 Gas analysis

The outlet of the headspace of the columns was directly connected to a gas chromatograph (Shimadzu Nexis GC-2030) with a Barrier Discharge Ionization (BID) detector. This allowed a constant monitoring of CO_2 and N_2O (ones per h). The detection limit was 0.25 ppm N_2O and 261.9 ppm CO_2, with a precision of at least 1% and 0.7%, respectively. Note that these N_2O fluxes derived from GC analysis may include N_2O from processes other than denitrification and are thus referred to as the total net N_2O fluxes. To analyze the isotopic composition of N_2O and N_2, samples were manually collected into 12 mL Exetainers® (Labco Limited, Ceredigion, UK) at intervals of 1, 2, 5, and 8 days during the incubation period. To remove residual air, each 12-mL exetainer was purged with helium (Helium 6.0, supplied by Praxair, Düsseldorf, Germany) three times, followed by air evacuation down to 40 mbar. The exetainers were then flushed with headspace gas from incubated columns for 20 minutes, achieving an eightfold exchange of the exetainer's volume with the gas. Additionally, after the incubation period, a sample of the technical gas was collected to assess the isotopic signature of the carrier gas. These gas samples were analyzed for isotopic signatures with an automated gas preparation and introduction system (GasBench II, Thermo Fisher Scientific, Bremen, Germany; modification based on Lewicka-Szczebak et al., 2013) connected to an isotope ratio mass spectrometer (MAT 253, Thermo Fisher Scientific, Bremen, Germany). This setup was used to measure the mass-to-charge ratios (m/z) of 28 ($^{14}N^{14}N$), 29 ($^{14}N^{15}N$), and 30 ($^{15}N^{15}N$) for N_2, and thus to simultaneously determine the isotope ratios of ^{29}R ($^{29}N_2/^{28}N_2$) and ^{30}R ($^{30}N_2/^{28}N_2$). We refer to Rohe et al. 2021 for details of measurement and concentrations as well as fractions of different pools

(i.e. concentration of N in N_2O (fp_{N_2O}) or N_2 (fp_{N_2}) and corresponding fraction of N in N_2O (Fp_{N_2O}) originating from ^{15}N labeled NO_3^- pool) as well as corresponding ap-values, i.e. the enrichment of ^{15}N in the $NO_3{}^-$pool undergoing denitrification. The product ratio of denitrification [N_2O / (N_2O + N_2)] was calculated for each sample:

$$product\ ratio\ = \frac{fp_{N_2O}}{fp_{N_2O} + fp_{N_2}} \tag{1}$$

The calculated average product ratio [N_2O / (N_2O + N_2)] of each treatment was also used to calculate the average total denitrification fluxes (N_2O + N_2 fluxes) during the incubation in $\mu g\ N\ h^{-1}\ kg^{-1}$:

$$N_2O + N_2 = \frac{fp_{N_2O}}{product\ ratio}. \tag{2}$$

Last, the sum of CO_2 and N_2O with a global warming potential of 298 was used for converting N_2O to CO_2-eq. was used to calculate the cumulative GHG production rate as CO_2-equivalents (CO_2-eq). We did not consider CH_4 production, as the GC chromatograms did not indicate any significant CH_4 emissions.

2.4 X-ray CT scanning and subsampling

After the experiment, the entire 10 cm Ø columns were X-ray CT scanned at 60 μm resolution (O_2-microsensors still attached). After this, four intact subsamples with 3 cm Ø and 3 cm height (stiff PVC sleeves with a wall thickness of 2 mm) were taken to be scanned at higher resolution (19 μm). These subsamples were extracted with a subsampling device (UGT GmbH, Germany) in two depths (2-5 cm and 6-9 cm). X-ray CT was conducted using an X-tek XTH 225 (Nikon Metrology) with an Elmer-Perkin 1620 detector panel (1750 × 2000 pixels). Imaging settings for the large cores were 190 kV, 330 μA, 1.5 mm Cu filter, 2800 projections, two frames per projection, while for the 3 cm cores 130 kV, 150 μA, 0.5 mm Cu filter, 2500 projections, and two frames per projection was used.

2.5 Image segmentation and analysis

Image segmentation and analysis were conducted using different plugins in Fiji (Schindelin et al. 2012). In short, the images were segmented into air-filled and water-filled pores, stones, and soil matrix using the machine learning plugin LABKIT (Arzt et al. 2022) along the lines of Lucas, Nguyen, et al. 2022. A visual examination of the images indicated that there was no over-segmentation of POM particles. Due to the resolution limit (19 μm), small POM particles may not be detected. Nonetheless, these smaller particles appear to be uniformly spread within the soil matrix according to Schlüter, Leuther, et al. 2022, suggesting that their distribution is not adversely affected in the overall POM analysis. Note, that here POM refers to all organic residues visible in the X-ray CT scan, i.e. also relatively fresh, but dead root residues cut during sampling. To further elucidate, if the distribution of fresh roots is different from the one of POM, we segmented roots from the total POM as written in Lucas, Gil, et al. 2023. In short, all POM particles, which were connected to the outer boundary of the image and were larger than 10.000 voxels, i.e. approx. 0.06 cm^3 were segmented as ”fresh” roots.

After segmentation, we used the Euclidean Distance Transform (Fig. 1) in Fiji to calculate the potential anaerobic volume, i.e. air distance larger than a threshold similar to Rohe et al. 2021. For this, unconnected air-filled pores were excluded from the pore image by “connected components labeling” and the “keep largest” method of the plugin MorphoLibJ (Legland et al. 2016, Version 1.4.3) after adding a white slice on top of the image. In this way, all pores connected to the top are kept and all isolated pores are removed. The distance threshold for potential anaerobic conditions was set based on sensitivity analyses before

further evaluation. For this, we computed linear regressions of the anaerobic volume resulting from varying distance thresholds of 0.06 mm - 5 mm with the N_2O+N_2 fluxes and minimized the *p*-value. We also used the distance maps to calculate the distance of POM to air-filled macropores within the subsamples similar to Ortega-Ramírez et al. 2023 and Lucas, Gil, et al. 2023. The same sensitivity analysis as for the anaerobic soil volume was conducted to estimate the distance threshold. We refer to all POM at higher distances as this threshold as occluded POM, while the POM within or close to air-filled pores is denoted here as free POM. There was no significant effect of the land use, so only one regression line was computed. Note that the traditional definitions of free and occluded POM, while often defined operationally by the fractionation method (Leuthold et al. 2023; Wagai et al. 2009), are similar to the here-defined free and occluded POM. Specifically, free POM is believed to be found in macropores between soil aggregates, while occluded POM is embedded within these aggregates, providing it with a degree of protection (Brodowski et al. 2006; Golchin et al. 1994; Kölbl et al. 2005).

2.6 Construction of a 3D O_2-map

The 3D Euclidean distance map of air-filled pores calculated for the large cores was also used to derive the exact positions of the sensor tips relative to air-filled pores within the 10 cm samples. After this, we conducted linear regression analysis for the two land uses in which the distance at each of the seven sensor tips per core was correlated with the O_2 saturation on the last day of the incubation. We choose to use the O_2 saturation at the end of the incubation to ensure that it aligns best with the structural information derived from X-ray CT scans directly after the incubation. The resulting models were used to compute the O_2-saturation of all voxels of the X-ray CT scan, i.e. at all possible distances to air-filled pores (Fig. 1).

2.7 ^{15}N-NO_3^- and ^{15}N-NH_4^+ analysis

During subsampling of the larger cores, disturbed soil samples at three different depths (1-3 cm, 5-6 cm, and 8-9 cm) were taken. 10 g fresh soil was extracted with 40 ml 1 M $K_2 2SO_4$solution (corresponds roughly to a ratio of 1:5 solid:liquid in relation to dry matter). After shaking for 1h, the mixture was centrifuged for 30 min at 3000 rpm. The supernatant was analyzed for $NH_4{}^+$-N and $NO_3{}^-$-N concentrations and ^{15}N-enrichment in $NH_4{}^+$ and NO3- using the SPINMAS technique (Stange et al. 2007). The measurements were carried out in an automated sample preparatory for inorganic nitrogen (SPIN unit; InProcess, Bremen, Germany) coupled with a mass spectrometer (GAM 400; InProcess, Bremen, Germany). For analysis of nitrate ca. 1 ml V(III)Cl_3 solution in an acidic medium (HCl) was added to a 5 ml sample at 85°C to reduce the $NO_3{}^-$ to NO and the m/z values 30 and 31 were measured. To calculate the ^{15}N abundance, the m/z value 31 was corrected, due to the interference of $^{14}N^{17}O$ (natural abundance of ^{17}O 0.037 at%) with $^{15}N^{16}O$. The quantification limit of $NO_3{}^-$ was 0.005 mmol/L. For analysis of ammonium ca. 1 ml bromate ($BrO_3{}^-$) in a sodium hydroxide (NaOH) solution was added to a 5 ml sample at 65°C to oxidize $NH_4{}^+$ to N_2. To calculate the ^{15}N abundance of $NH_4{}^+$, the m/z values 28, 29, and 30 were measured. The quantification limit of $NH_4{}^+$ was 0.03 mmol/L

2.8 Statistics

For all statistical analysis, the software R 4.3.1 (R Core Team 2023) in combination with the package agricolae (Mendiburu et al. 2020) was used. Differences in the data were revealed with a two-factorial ANOVA with the factors of land use (grassland vs. cropland) and moisture content (-160 cm, -40 cm, and -8 cm matric potential). When the interactions between the studied factors were found to be statistically significant (p <0.05), the least significant difference (LSD) tests were applied. The assumptions of normality and homogeneity of variances were assessed using normal probability plots of the residuals and

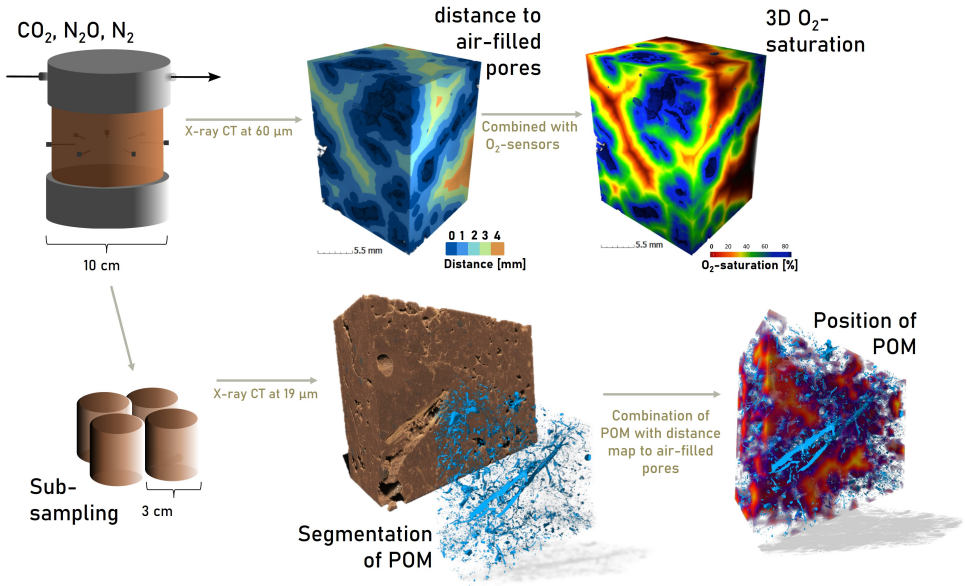

Figure 1. Experimental setup and imaging workflow. The incubation is conducted with 10 cm soil cores under a constant flow of a technical gas with 21% O_2 and 0.5% N_2. The entire cores were X-ray CT scanned and analyzed according to the top row, i.e. Euclidean distance maps were derived to examine the exact position of the O_2-sensor tips. A linear correlation of these distances with the O_2 measurements allowed us to construct a 3D map of O_2 saturation. In addition, subsamples of 3 cm size enabled the segmentation of POM at high resolution and to derive its distribution in the heterogeneous soil matrix (bottom row).

Levene's tests for equal variances, respectively. To address our research question concerning evaluating soil structural properties as predictors of denitrification, we computed linear regression models of these with the fluxes of N_2O, N_2O+N_2, CO_2, and GHG.

3 RESULTS

3.1 Gasfluxes

The CO_2 and total N_2O emissions over time exhibited considerable variability among the tested soil cores, even among those sharing the same land use type and moisture level (Fig. S1). Notably, there was a distinct land use-dependent influence on CO_2 emissions, with the grassland demonstrating significantly higher CO_2 emissions under drier conditions compared to the cropland, particularly at matric potentials of -160 cm (528,3 g C $kg^{-1}h^{-1}$in the grassland compared to 190,0 g C $kg^{-1}h^{-1}$in the cropland) and -40 cm (Fig. 2a, 532,8 g C $kg^{-1}h^{-1}$in the grassland compared to 200,0 g C $kg^{-1}h^{-1}$in the cropland). Conversely, N_2O emission (Fig. 2b) and combined N_2O+N_2 fluxes (Fig. 2c) exhibited an increase with moisture, showing no discernible difference under drier conditions but higher emissions from the grassland under the wettest conditions tested. At the drier matric potentials, grassland samples featured significantly higher product ratios of N_2O and N_2 emissions (0.60 at -160 cm and 0.53 at -40 cm pressure head) compared to cropland (0.30 at -160 cm and 0.27 at -40 cm pressure head, Fig. 2d). Yet, these differences diminished, with both land use types showing comparable levels at a matric potential of -8 cm (0.68 for the grassland and 0.63 for the cropland). Thus, at wet conditions, almost no N_2O produced during denitrification was further reduced to N_2.

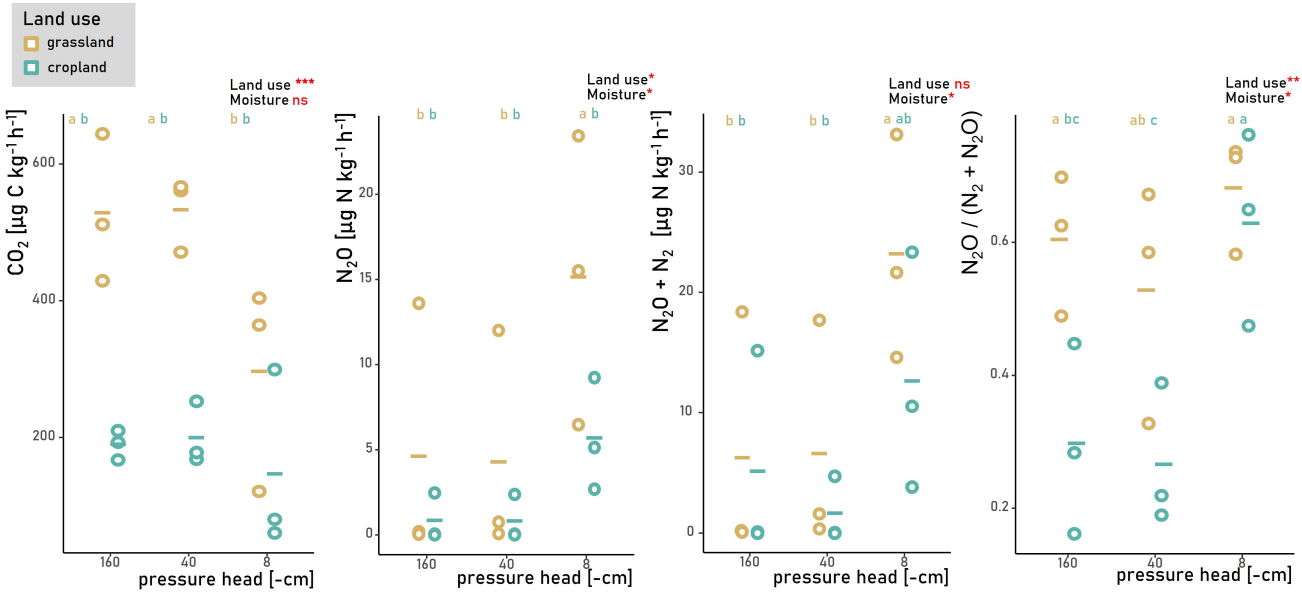

Figure 2. Gas fluxes during the incubation period for the two land uses at three different moisture contents. Shown are the mean fluxes of a core (circles) and the mean of the treatment (crossbar) for A) CO_2, B) N_2O, C) N_2O+N_2, and D) the product ratio of N_2 and N_2O. of the two land uses N_2O+N_2. Different letters in A-D indicate significant differences as derived from an LSD test (n=3, p value <0.05). In addition, we report significant effects of the land use (grassland vs. cropland) and of soil moisture (matric potential of -160 cm vs. -40 cm vs -8 cm matric potential) and marked by ns, *, **, and *** for p values >0.05, <0.05, <0.01, and <0.001, respectively.

However, the proportion of N_2O derived from denitrification (Fp_{N_2O}) consistently exceeded 0.6, approaching values close to one and unity at -8 cm matric potential (Fig. S2b). The calculated enrichment of ^{15}N in the nitrate pool undergoing denitrification (ap-values) was significantly greater in the grassland across all moisture levels (Fig. S2a), corroborating the trends observed in the measured ^{15}N values of extracted nitrate (Fig. S2D) and ammonium (Fig. S2E), which aligned well with these enrichment data (Fig. S2G). This agreement in the data underlines the homogeneity of the ^{15}N labeling as it shows that the ^{15}N enrichment of NO_3^- in anoxic microsites was identical with the ^{15}N enrichment of extracted soil nitrate. NO_3^- concentrations after incubation did not significantly vary by land use or moisture conditions (Fig. S2C). Yet, the numerically lowest NO_3^- concentrations were noted under the wettest conditions tested, aligning with the observed increase in N_2O+N_2 fluxes. The NH_4^+ concentration in none of the samples exceeded the quantification limit of 0.02 mmol/L, roughly corresponding to <5 µg/g soil.

3.2 Explanatory variables derived from X-ray CT

3.2.1 Distance to air-filled pores

Sensitivity analyses revealed threshold distances almost identical for the cropland and the grassland (Table 1, 0.9 and 1.02, respectively), which were used to calculate the potential anaerobic volume, i.e. the soil volume that is further away from air-filled pores (Table 1). Under dry conditions, in which the majority of macropores are air-filled (Table S1), occurrences of distances to air-filled pores exceeding 1 mm were nearly nonexistent (Fig. S3). Increasing moisture content generally led to larger distances (Fig. S3). Correspondingly, the potential anaerobic soil volume exhibited an increasing trend from the driest to the wettest soil, with numerically higher values observed in the cropland caused by distinct differences in the

pore structure between the two land uses (Fig. 3b). However, notable outliers were observed in the grassland soil, with some cores displaying high potential anaerobic volumes, emphasizing the heterogeneity in the field. In the case of the grassland, there was a strong association between the potential anaerobic volume and the N_2O+N_2 fluxes (Fig. 3a, R^2=0.82, p<0.001). For the cropland, however, this association was not significant (p>0.05), and even samples with relatively high potential anaerobic soil volumes resulted in fluxes of N_2O+N_2 close to 0. Note that the potential anaerobic volume is based on 3D pore distances only and is therefore a proxy for O_2 supply without information about the heterogeneous distribution of O_2 demand.

3.2.2 3D oxygen distribution

In addition to monitoring greenhouse gas fluxes, we tracked O_2 in % air saturation using microsensors throughout the experiment (Fig. S4). The majority of these microsensors consistently indicated air saturation levels close to 100% throughout the entire incubation period, with only a few registering values below 50% at the onset of the experiment and thereafter. Under wetter conditions (-8 cm), there was a collective decrease in O_2 readings over time, although saturation levels never approached zero. The O_2 saturation at the end of the incubation displayed a significant correlation with the distance to air-filled pores as computed for the sensor tips (Fig. S7), albeit with some outliers showing relatively low O_2 saturation at shorter pore distances.

Based on these associations, we derived the 3D distribution of O_2 (Fig. 1) along with corresponding average values (Fig. 3d). In comparison to the potential anaerobic soil volume, the average O_2 saturation was less affected by soil moisture, and contrary to expectations based on the potential anaerobic soil volumes, the cropland exhibited higher rather than lower O_2 saturation levels compared to the grassland (78.3% in the cropland and 71.3% in the grassland). Additionally, the average 3D O_2 saturation displayed a strong negative correlation with N_2O-N_2 fluxes (R^2=0.52, p<0.001) and was unaffected by land use type (Fig. 3c).

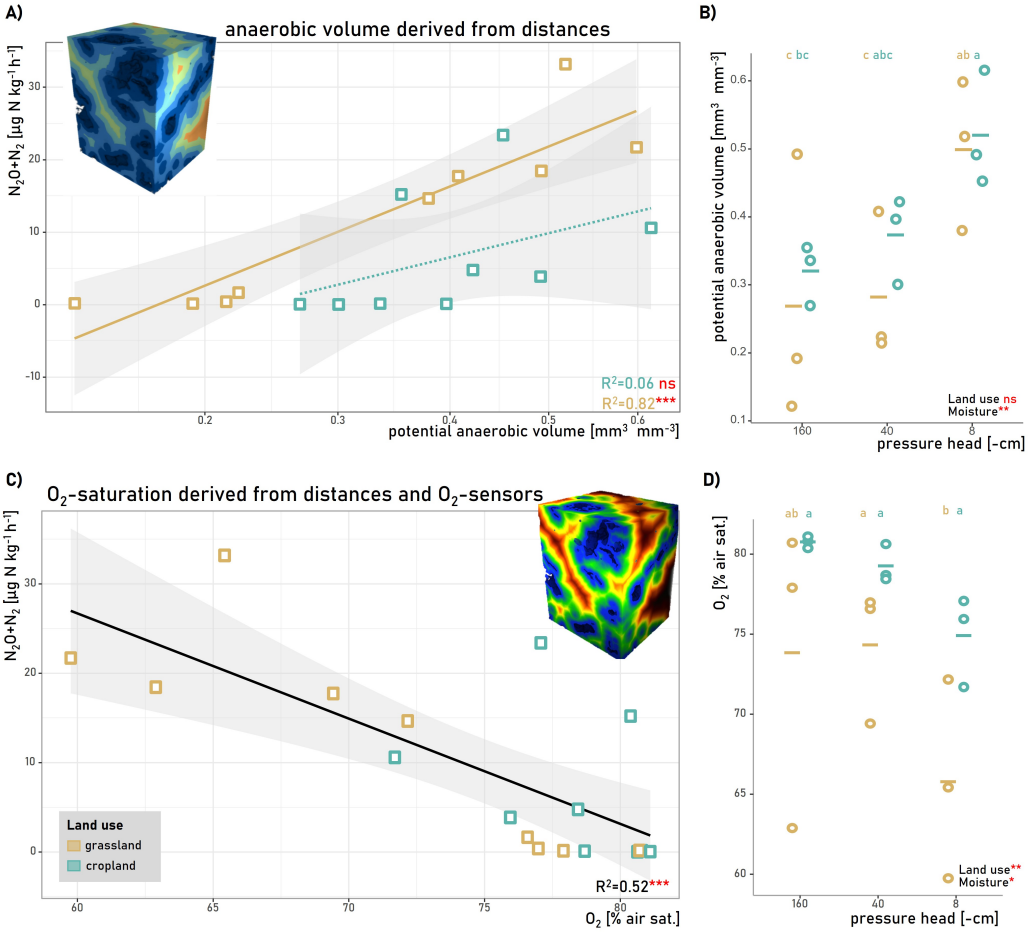

Figure 3. The anaerobic volume as a driver of denitrification. A) Association of the potential anaerobic soil volume (derived from X-ray CT) with N_2O+N_2 and B) respective mean volumes of a soil core (circles) and the mean of the treatment (crossbar) for the two different land uses and the three investigated water potentials of the potential anaerobic soil volume. C) Association of the mean O_2-concentration in % of air saturation of the soil core (derived by a combination of X-ray CT and microsensors) with N_2O+N_2 fluxes and D) respective mean O_2-concentration of a soil core (circles) and the mean of the treatment (crossbar) for the potential anaerobic soil volume. The solid lines in A) and C) represent fitted linear models. Respective R^2 and significance level are given in the corner of the graphs. Different letters in B and D indicate significant differences as derived from an LSD test (n=3, p value <0.05). In addition, we report significant effects of the land use (grassland vs. cropland) and of soil moisture (matric potential of -160 cm vs. -40 cm vs -8 cm) marked by ns, *, **, and *** for p-values >0.05, <0.05, <0.01, and <0.001, respectively.

3.2.3 Position of POM

We enhanced the resolution of X-ray CT scanning by subsampling the incubated cores, enabling the segmentation of POM (Fig. 1). Consistent with the higher total carbon concentration in grassland, we observed a significantly higher share of POM in the grassland (4.0-4.6%) compared to the cropland with values ranging between 1. and 2.7% (Table S1). The distribution of POM was strongly skewed towards small air distances, with nearly all POM situated within or close to air-filled pores (Fig. S3a). Thus, for both land uses, the mean air distance of the POM in relation to air distances of the soil matrix was ¡0.1. However, this distribution indicator revealed consistently higher values in the grassland than in the cropland indicating a better incorporation of POM into the soil matrix within the grassland (grassland: 0.031 - 0.045,

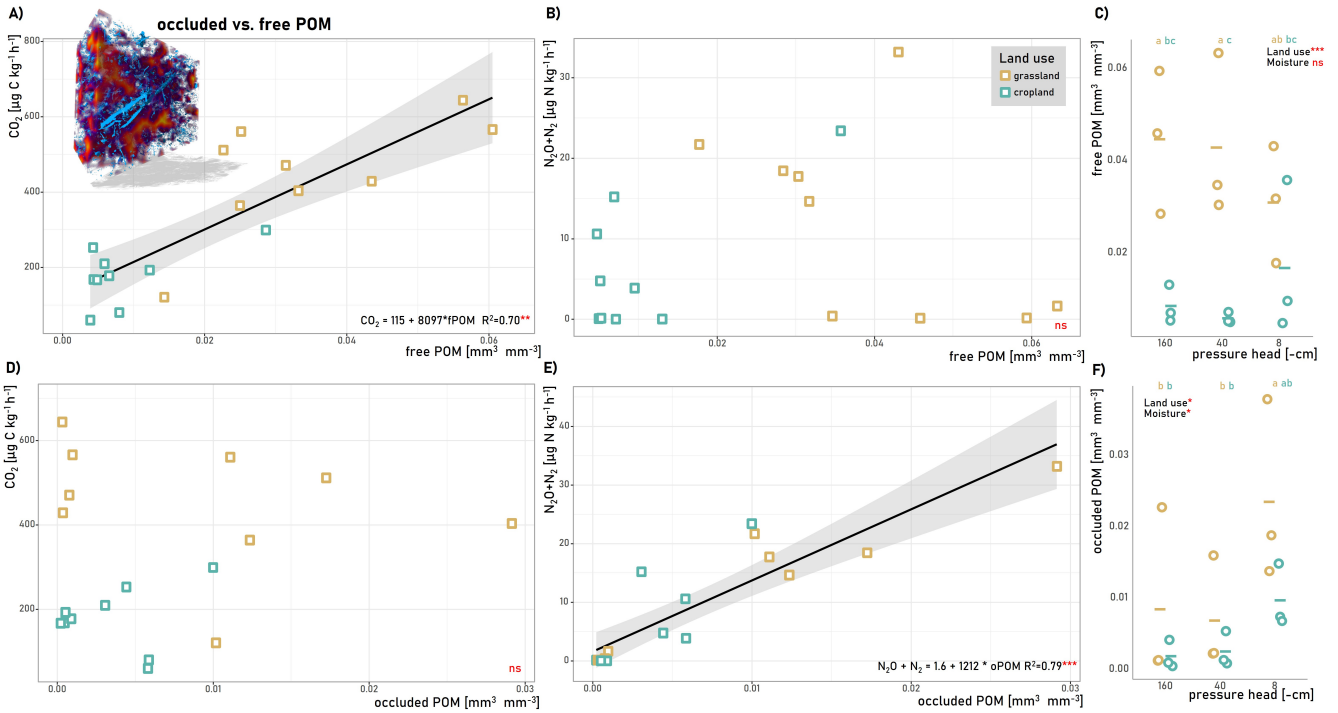

Figure 4. The position of POM as the driver of denitrification. Association of the amount of free POM and CO_2 fluxes (A), N_2O+N_2 fluxes produced through denitrification (B), and respective mean values of the amount of free POM volume (C) for the two different land uses and the three investigated water potentials. Association of the amount of free POM as well as occluded POM with CO_2 fluxes (A, C), N_2O+N_2 fluxes (B, E), and respective mean values of the amount of the free POM volume (C), and the occluded POM volume (F) for the two different land uses and the three investigated water potentials. The solid lines in A), B), D), and E) represent fitted linear models. Respective R^2 and significance level are given in the corner of the graphs. Different letters in B and D indicate significant differences as derived from an LSD test (n=3, *p* value <0.05). In addition, we report significant effects of the land use (grassland vs. cropland) and of soil moisture (matric potential of -160 cm vs. -40 cm vs -8 cm) marked by ns, *, **, and *** for *p*-values >0.05, <0.05, <0.01, and <0.001, respectively.

cropland: 0.01 - 0.02, Fig. S3b). However, as moisture content increased and some macropores containing POM filled with water (Table S1), distances of POM to pores increased relative to the matrix distances. Interestingly, the portion of POM identified as relatively fresh roots exhibited a similar pattern, with most roots located within or close to air-filled pores (Fig. S5). The volume of free POM, defined as POM closer than 0.59 mm to air-filled pores as indicated by sensitivity analysis related to N_2O+N_2 fluxes, showed no significant variation with soil moisture but was higher in grassland than in cropland (Fig. 4c, 0.04 mm^3 mm^{-3} compared to 0.01 mm^3 mm^{-3}). On the other hand, occluded POM, increased with moisture content and was higher in the grassland across all moisture conditions (Fig. 4f). While free POM did not show a significant correlation with N_2O+N_2 fluxes from denitrification, it was strongly associated with CO_2 fluxes (R^2=0.7, *p* value<0.001, Fig. 4a,b). In contrast, occluded POM displayed the opposite pattern, with a strong association with N_2O+N_2 fluxes produced by denitrification (R^2=0.79, *p* value<0.001) and no association with CO_2 fluxes (Fig. 4d,e). The association of the occluded POM with N_2O alone was even stronger (R^2=0.90, *p* value <0.001, Fig. S6) compared to N_2O+N_2. Additionally, the amount of occluded POM displayed a clear negative correlation with NO_3^- concentrations, in accordance with its link to denitrification processes (S2f).

3.2.4 CO_2 equivalents

We found compelling associations between the POM volume and GHG production quantified as the CO_2-equivalents of CO_2 and N_2O combined (Fig. 5a). Building upon our previous findings for N_2O and CO_2 alone, we observed that both free POM and occluded POM exhibited universal, linear relationships across land uses and water contents with GHG production. Notably, occluded POM demonstrated a steeper increase in association with GHG production, reflecting its role in the heightened production of the more potent greenhouse gas N_2O. Furthermore, GHG production displayed significant associations with both land use type and moisture content. The grassland consistently exhibited numerically higher GHG production compared to the cropland across all moisture conditions (5.26 mg CO_2-eq kg^{-1} h^{-1} in the grassland and 1.79 mg CO_2-eq kg^{-1} h^{-1} in the cropland). This result aligns with our previous findings regarding the association of free POM with CO_2 and occluded POM with N_2O, leading to the highest CO_2-equivalents in the wettest grassland soil cores, when most of the POM becomes occluded.

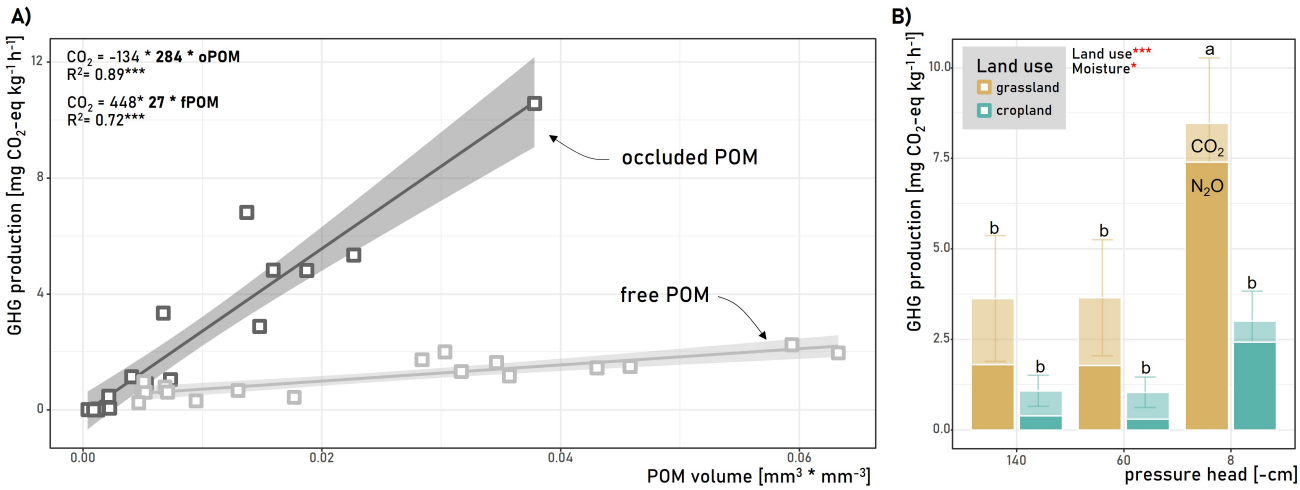

Figure 5. Impact of the share of free POM and occluded POM on the production of GHG (CO_2 equivalents of CO_2 and N^2O) (A) and respective mean values and standard deviations for the two different land uses and the three investigated water potentials. The solid lines represent fitted linear models. Respective R_2 and significance level are given in the corner of the graphs. Different letters in B indicate significant differences as derived from an LSD test (n=3, *p*-value <0.05). In addition, we report significant effects of the land use (grassland vs. cropland) and of soil moisture (matric potential of -160 cm vs. -40 cm vs -8 cm) marked by ns, *, **, and *** for *p*-values >0.05, <0.05, <0.01, and <0.001, respectively.

3.2.5 Comparison to sieved soil

The comparison between repacked soil cores used in Rohe et al. 2021 and the structured soil cores in our study revealed notable differences in the estimated distance thresholds used to calculate the potential anaerobic volume, with much lower distance thresholds in the structured cores (Table 1). Surprisingly, despite these differences, the potential anaerobic volume averaged across all three moisture contents did not show significant differences between the sieved and structured versions of the soil. However, significant disparities emerged in the O_2-saturation calculated from the microsensors installed. In the repacked soil, grassland cores exhibited a mean O_2 saturation of 49.0±13.6%, and cropland cores showed 48.1±15.98%. In contrast, the structured cores displayed significantly higher O_2 saturation, with grassland at 72.3±20.8% and cropland at 75.7±11.7%. Despite the higher O_2 saturation in structured cores, N_2O, N_2O+N_2, CO_2

fluxes, and the product ratio of N_2O and N_2 were consistently higher in the grassland compared to cores from the cropland, regardless of whether they were sieved or structured.

Table 1. Mean values and standard deviation for basic parameters of the two land uses under field structured conditions in comparison to sieved soil as presented in Rohe et al. (2021) (n=3 moisture contents). The distance threshold describes the minimum distance to air-filled pores after which the soil was denoted as anaerobic and is the result of linear regression analysis of the association of N_2O+N_2 with X-ray CT-derived information.

	grassland		cropland	
	repacked	structured	repacked	structured
distance threshold [mm]	5	1.02	5	0.9
potential anaerobic volume [cm3 cm-3]	0.32±0.42a	0.35±0.13a	0.31±0.37a	0.40±0.1a
O_2 [% air-sat.]	48.97±13.55b	72.28±20.78a	48.1±15.98b	75.73±11.71a
N_2O [µg N kg^{-1} h^{-1}]	11.37±9.75a	8.01±8.54ab	3.37±2.88bc	2.44±3.1c
CO_2 [µg C kg^{-1} h^{-1}]	435.29±203.62a	433.29±142.84a	126.67±53.94b	182.49±79.24b
N_2O+N_2 [µg N kg^{-1} h^{-1}]	18.21±12.57a	12.01±11.97ab	5.75±5.12b	6.46±8.32b
N_2O / (N_2O+N_2)	0.57±0.23a	0.6±0.13a	0.45±0.3b	0.4±0.21b

4 DISCUSSION

In this study, we investigated the dynamics of CO_2, N_2, and N_2O emissions, in soil cores under varying moisture conditions and land use types. Utilizing a combination of gas flux measurements, microsensor data, and X-ray CT scanning, we sought to understand the underlying mechanisms driving the production of these gases and their relationship with soil properties. Our findings revealed significant variability in CO_2, N_2 and N_2O emissions and in the fraction of N_2O from denitrification across different land use types and moisture levels (Fig. 2). Moreover, our investigation into POM distribution highlighted its influence on GHG production, with both free and occluded POM showing associations with CO_2, N_2 and N_2O fluxes, respectively (Fig. 5).

4.1 Denitrification induced by POM

Similar to previous studies, our analysis of the 3D O_2 distribution demonstrated the direct and decisive influence of O_2 on N_2O in structured soils (Du et al. 2023; Song et al. 2019; Wei et al. 2023, Fig. 3). In addition to these studies, however, we also analyzed N_2 to get an estimate of the complete potential of N losses through denitrification. The extent of denitrification in soils is a result of balancing between O_2 demand and supply (G P Robertson 2023; Rohe et al. 2021). The O_2 supply, on the one side, is controlled by the soil structure through the regulation of diffusion distances and the establishment of potential anaerobic volumes (Du et al. 2023; Lucas, Gil, et al. 2023; Rohe et al. 2021, Fig. 3). Optimal soil moisture conditions for intensive N_2O emissions typically fall within a broad range of around 70% water-filled pore space (WFPS), with variations observed among different land uses (Bateman et al. 2005; Rohe et al. 2021; Ruser et al. 2006; Weier et al. 1993) This variability can be attributed to the emergence of anaerobic soil volumes in hotspots of high oxygen consumption within an otherwise well-aerated soil. This work emphasizes the need to precisely pinpoint the other side of the O_2 balance, i.e. the O_2 demand, to gain a better understanding of the denitrification potential by assessing the distribution of these hotspots. This is because the distribution of POM within the heterogeneous pore system is a key determinant of denitrification rates in structured soils. While for POM close or within air-filled pores the enhanced O_2 demand can mostly be

satisfied and predominately CO_2 is produced, it is the anaerobic microsite formed on occluded POM, where all factors for denitrification, i.e. low O_2, high C, and N are met (Fig. 4). This is in agreement with findings revealing that large mean distances of POM to air-filled pores are associated with N_2O emissions (Lucas, Santiago, et al. 2023; Ortega-Ramírez et al. 2023). The significance of POM as a hotspot for denitrification is further highlighted through the comparison with the sieved soil studied in Rohe et al. 2021. Our findings reveal a stark contrast in the threshold for oxygen limitations, which was observed to exceed 5 mm in sieved soils lacking POM, as opposed to the approximately 1 mm threshold in naturally structured field soils (Table 1). This discrepancy underscores the limited capacity for denitrification initiation within soil matrices devoid of POM hotspots, given the need for diffusion length >5 mm to exceed the relatively low O_2 demand — a condition scarcely met in structured field soils even under conditions of low matric potential (Fig. S3). Last, the role of occluded POM in the fate of NO_3^- is supported by the observed correlation between areas with low NO_3 concentrations and those with high levels of occluded POM (Fig. S2). In conclusion, to refine predictions of denitrification processes, future models should include particulate organic matter (POM) as a dynamic state variable and parameterize the occlusion of POM relative to soil moisture content. Note that the linear relationship between occluded POM and N_2O+N_2 produced by denitrification found in this study was unaffected by land use. This holds promise for the development of a universal empirical equation and could significantly enhance the predictive accuracy of denitrification models. Note, that the CT-based identification of particulate organic matter (POM) fractions marks a significant advancement over the traditional density fractionation method for categorizing occluded and free POM as hotspots of denitrification and aerobic respiration, respectively. This is due to the dynamic nature of CT-derived POM fractions, whose proportions fluctuate with changes in water content, as illustrated in Figure 4c. This fluctuation enables a more accurate prediction of denitrification by capturing the interplay between oxygen demand and supply, under varying moisture levels. Consequently, there is a compelling case for further investigation to develop comparably effective denitrification predictors that integrate the methodological simpler occluded POM determination through fractionation with pore structural measures, such as pore size distribution.

4.2 Denitrification in cropland vs. grassland

The investigated grassland and cropland featured different pore structures and POM abundances (Fig. 6). Notably, despite larger potential anaerobic volumes brought about by pore structure (3b), the cropland had higher O_2 saturation and lower denitrification activity because of lower POM content in general, and lower occluded POM content in particular (Table 1). Thus, the position of POM in the cropland, often near or within pores, limited denitrification rates despite the dense structure. This configuration resulted in relatively low denitrification rates compared to the grassland, where the abundance of occluded POM was notably higher (Fig. 4 and Fig. 5b). The reason for this is that POM is largely derived from roots that tend to grow into macropores (Lucas, Nguyen, et al. 2022; Lucas, Schlüter, et al. 2019a; White et al. 2010, Fig. S5), and thus POM fragments are typically located close to air-filled macropores (Kravchenko, Guber, et al. 2018; Schlüter, Leuther, et al. 2022). Conversely, the grassland, characterized by its lower bulk density (Table 1) and higher SOC content, presented a contrasting scenario with reduced potential anaerobic volumes and consequently enhanced O_2 supply, particularly under dry conditions (3). However, the advantage in O_2 supply was offset by the higher O_2 demand attributed to the substantial amounts of POM present in the grassland (Table S1). Under dry conditions, microbial respiration primarily drove the utilization of this POM, especially within or proximate to macropores. Thus, the grassland exhibited higher CO_2 fluxes, while under drier conditions N_2O fluxes were similar to those in the cropland. As moisture levels increased and macropores became increasingly saturated, the saturation of these hotspots led to a

reduction in O_2 supply. Consequently, the accumulation of large amounts of occluded POM under moist conditions triggered N_2O emissions and consequently the overall GHG production (Fig. 5). The more evenly distributed POM in the grassland compared to the cropland (S3b) led to the high association of N_2O+N_2 emissions with CT-derived potential anaerobic soil volumes (Fig. 3). This shows that in soils with an even distribution of hotspots (oxygen demand), the reason for heterogeneity in denitrification is the variation of oxygen supply at the microscale (Lucas, Gil, et al. 2023; Rohe et al. 2021)). However, our observations underline the major importance of denitrification for the total N_2O emissions from soil, particularly under near saturated conditions when N_2O production rates were high and almost all N_2O is produced by denitrification (Fig. S2b), corroborating previous findings (Gao et al. 2023; Liang et al. 2021; Lucas, Gil, et al. 2023; Ostrom et al. 2021). In addition, the sustained N_2O emissions observed even after 10 days of incubation support the notion, that hotpots of N_2O can persist for several weeks under static conditions (Christensen et al. 1990). However, denitrification completeness, often expressed by the product stoichiometry, $N_2O/(N_2O+N_2)$, can vary a lot in soils depending on environmental factors. Rohe et al. 2021 suggested that large diffusion distances of N_2O through the soil matrix favor N_2O reduction. However, the structured cores used in this study had the same product ratio of N_2O and N_2 compared to the sieved soils despite much higher diffusion distances (Table 1). This suggests that diffusion distance does not exclusively control this ratio. The disparity in soil pH levels offers a plausible explanation for the observed differences in product ratios (2d) among the land uses examined (Čuhel et al. 2011). Yet, under the wettest conditions, both land use types exhibited similarly high product ratios (>0.6), indicating a shift towards N_2O under high denitrification rates - this phenomenon, although noted before (Kemmann et al. 2021; Lucas, Santiago, et al. 2023) is controversial to the basic understanding of denitrification, where decreased O_2 concentration leads to an increase of N_2O reductase (NOS) and thus to more N_2 (Morley et al. 2010; G Robertson et al. 2024). A potential explanation, awaiting experimental validation, emerges from observations of the model denitrifier Paracoccus denitrificans, which under hypoxic conditions synthesizes nitrous oxide reductase (NOS) in all cells, whereas other enzymes in the denitrification pathway are scarcely expressed (Lycus et al. 2018). This bet-hedging strategy is thought to be common among denitrifying bacteria and may lead to NOS activity under moderate moisture conditions characterized by multiple oxic and hypoxic microsites (Lycus et al. 2018). Conversely, under the wettest conditions tested, anoxic zones become more prevalent, prompting a stronger expression of nitrate and nitrite reductases and therefore N_2O emissions.

4.3 Concluding remarks

Our observations underscore the intricate interplay between soil pore structure, moisture dynamics, and POM distribution in modulating denitrification processes and greenhouse gas emissions. Moreover, they emphasize new possibilities in soil N management and mitigation strategies aimed at curbing greenhouse gas emissions from terrestrial ecosystems, which include strategies for changing the distribution of POM. Recent literature emphasizes the critical role of anoxic microsites in regulating CO_2 emissions (Keiluweit, Nico, et al. 2016; Lacroix, Aeppli, et al. 2023; Lacroix, Mendillo, et al. 2022). Keiluweit, Wanzek, et al. 2017 underscored the importance of oxygen limitation in soil domains with restricted oxygen supply, such as aggregates or peds, in modulating carbon storage dynamics. These studies collectively suggest that anoxic microsites are crucial in governing carbon storage in terrestrial ecosystems. Moreover, a recent perspective by Angst et al. 2023 emphasizes the need to consider the site-specific relevance of POM in carbon sequestration. These perspectives suggest that while matrix-associated organic matter accumulation has traditionally been a focus of carbon sequestration efforts, the persistence and significance of POM, particularly in its occluded form, should not be overlooked. Our findings align with this perspective, indicating that occluded POM in the soil matrix indeed is protected from microbial respiration and

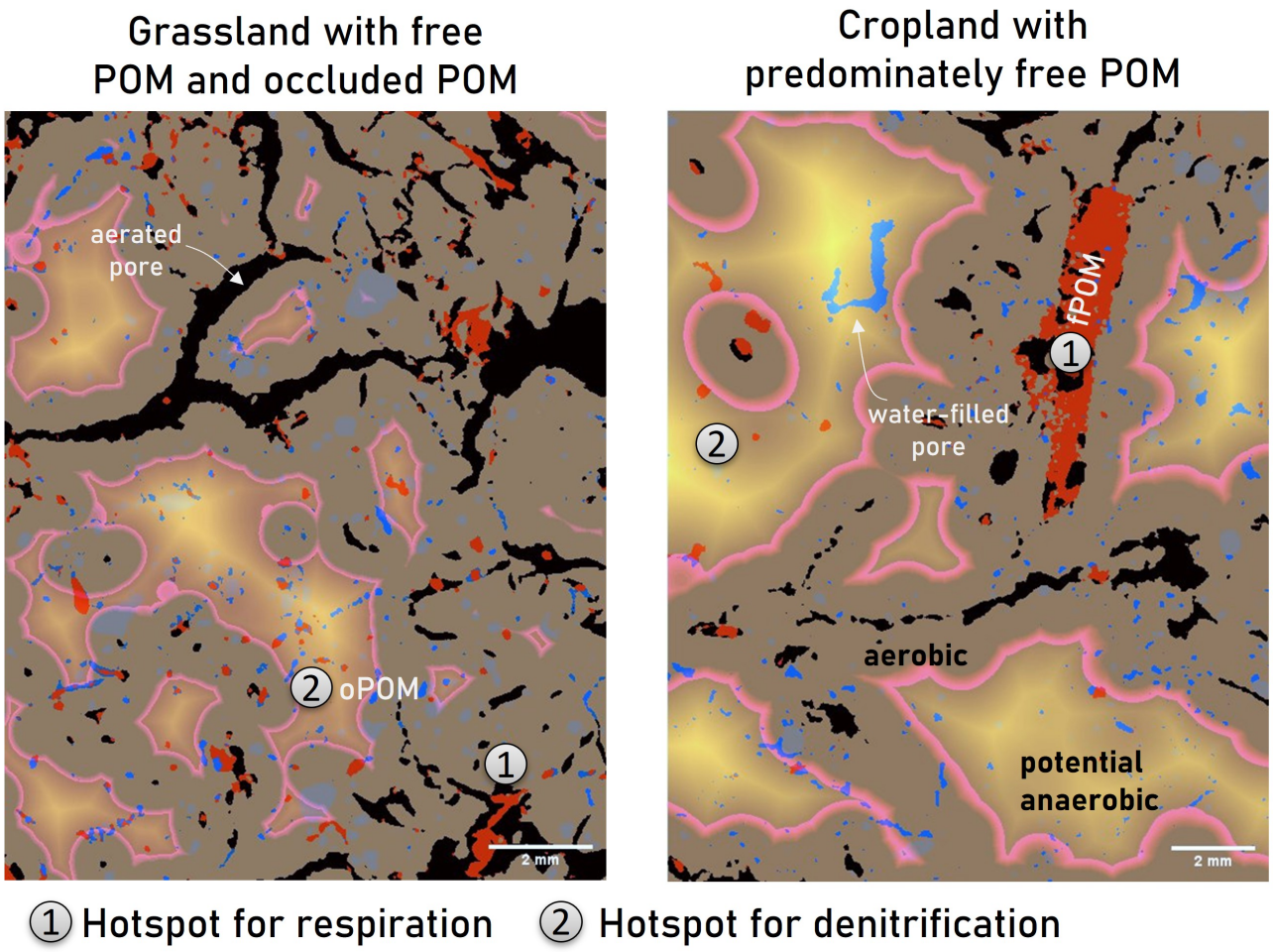

Figure 6. 2D slices of segmented X-ray CT images of the grassland and the cropland. The distribution of POM (red) to air-filled pores (black) is decisive for the formation of hotspots of denitrification vs. respiration. Hotspots of respiration are created by POM at low distances to air-filled pores, while POM in the potential anaerobic volume (yellow area) leads to a hotspot of denitrification. Note that, in the grassland the distribution of POM was more evenly in comparison to the cropland. The latter was characterized by the presence of large volumes of potentially anaerobic volumes, but relatively few hotspots (occluded POM) for denitrification in it.

therefore decreases CO_2 losses. However, the positive effects on the climate balance associated with measures to increase carbon storage in soils can be reduced or even negated by N_2O emissions (Guenet et al. 2021). Indeed, our data suggest the drawback in the overall climatic balance when storing POM in the soil matrix for C protection. Note that our incubation setups involved both, high moisture status and NO_3^--levels. These conditions may be met in heavily managed soils during high rain events. Therefore, as previously suggested by modelling results, such a risk of increased N_2O emissions from management practices targeting C accumulation can be mitigated by adjusting N fertilisation rates (Qiu et al. 2009; You et al. 2024)

CONFLICT OF INTEREST STATEMENT

The authors declare that the research was conducted in the absence of any commercial or financial relationships that could be construed as a potential conflict of interest.

AUTHOR CONTRIBUTIONS

ML and BA conducted the incubation experiment. RW analyzed the IRMS data. CFS conducted the SpinMas analysis. LR and BA conducted pre-experiments and optimized the incubation setup. SS, HJV, ML, RW, and LR conceived the experiment. ML did the combined data analysis. Funding acquisition by HJV and SS. All authors have seen and approved the final version submitted and were part of the writing process.

ACKNOWLEDGMENTS

This study was funded by the Deutsche Forschungsgemeinschaft through the research unit DFG-FOR 2337: Denitrification in Agricultural Soils: Integrated Control and Modeling at Various Scale (DASIM), grant number 270261188.

DATA AVAILABILITY STATEMENT

The datasets generated for this study can be found under the DOI:10.48758/ufz.14621.

5 REFERENCES

Angst, Gerrit, Kevin E. Mueller, Michael J. Castellano, Cordula Vogel, Martin Wiesmeier, and Carsten W. Mueller (2023) "Unlocking complex soil systems as carbon sinks: multi-pool management as the key". In: *Nature communications* 14.1, p. 2967. DOI: 10.1038/s41467-023-38700-5.

Arzt, Matthias, Joran Deschamps, Christopher Schmied, Tobias Pietzsch, Deborah Schmidt, Pavel Tomancak, Robert Haase, and Florian Jug (2022) "LABKIT: Labeling and Segmentation Toolkit for Big Image Data". In: *Frontiers in Computer Science* 4, p. 777728. DOI: 10.3389/fcomp.2022.777728.

Bateman, E. J. and E. M. Baggs (2005) "Contributions of nitrification and denitrification to N2O emissions from soils at different water-filled pore space". In: *Biology and Fertility of Soils* 41.6, pp. 379–388. DOI: 10.1007/s00374-005-0858-3.

Briones, María Jesús I. and Olaf Schmidt (2017) "Conventional tillage decreases the abundance and biomass of earthworms and alters their community structure in a global meta-analysis". In: *Global change biology* 23.10, pp. 4396–4419. DOI: 10.1111/gcb.13744.

Brodowski, S., B. John, H. Flessa, and W. Amelung (2006) "Aggregate-occluded black carbon in soil". In: *European Journal of Soil Science* 57.4, pp. 539–546. DOI: 10.1111/j.1365-2389.2006.00807.x.

Christensen, Søren, Stephen Simkins, and James M. Tiedje (1990) "Temporal Patterns of Soil Denitrification: Their Stability and Causes". In: *Soil Science Society of America Journal* 54.6, pp. 1614–1618. DOI: 10.2136/sssaj1990.03615995005400060017x.

Čuhel, Jiří and Miloslav Šimek (2011) "Proximal and distal control by pH of denitrification rate in a pasture soil". In: *Agriculture, Ecosystems & Environment* 141.1, pp. 230–233. DOI: 10.1016/j.agee.2011.02.016.

Diel, Julius, Hans-Jörg Vogel, and Steffen Schlüter (2019) "Impact of wetting and drying cycles on soil structure dynamics". In: *Geoderma* 345, pp. 63–71. DOI: 10.1016/j.geoderma.2019.03.018.

Du, Yanling, Shengli Guo, Rui Wang, Xiaotong Song, and Xiaotang Ju (2023) "Soil pore structure mediates the effects of soil oxygen on the dynamics of greenhouse gases during wetting–drying phases". In: *Science of The Total Environment* 895, p. 165192. DOI: 10.1016/j.scitotenv.2023.165192.

Firestone, Mary K. and E. A. Davidson (1989) "Microbiological basis of NO and N2O production and consumption in soil". In: *Exchange of trace gases between terrestrial ecosystems and the atmosphere: Report of the Dahlem Workshop on Exchange of Trace Gases between Terrestrial Ecosystems and the Atmosphere, Berlin 1989, February 19 - 24*. Ed. by M. O. Andreae. In collab. with Workshop on Exchange of Trace Gases between Terrestrial Ecosystems {and} the Atmosphere. Vol. 47. A Wiley Interscience publication. Chichester: Wiley, pp. 7–21. ISBN: 978-0-471-92551-4.

Fomin, Dmitriy S., Anna V. Yudina, Konstantin A. Romanenko, Konstantin N. Abrosimov, Marina V. Karsanina, and Kirill M. Gerke (2023) "Soil pore structure dynamics under steady-state wetting-drying cycle". In: *Geoderma* 432, p. 116401. DOI: 10.1016/j.geoderma.2023.116401.

Gao, Na, Fangfang Zhang, Qifei Bo, Tang, JiaRui Gao, Xiongxiong Wei, Shanchao Yue, Yufang Shen, and Shiqing Li (2023) "Microbial and isotopomer analysis of N2O production pathways in a calcareous film-mulched farmland". In: *Biology and Fertility of Soils* 59.4, pp. 407–422. DOI: 10.1007/s00374-023-01711-x.

Golchin, A Jm Oades, Jo Skjemstad, and P Clarke (1994) "Soil structure and carbon cycling". In: *Soil Research* 32.5, p. 1043. DOI: 10.1071/SR9941043.

Groffman, Peter M., Klaus Butterbach-Bahl, Robinson W. Fulweiler, Arthur J. Gold, Jennifer L. Morse, Emilie K. Stander, Christina Tague, Christina Tonitto, and Philippe Vidon (2009) "Challenges to incorporating spatially and temporally explicit phenomena (hotspots and hot moments) in denitrification models". In: *Biogeochemistry* 93.1, pp. 49–77. DOI: 10.1007/s10533-008-9277-5.

Guenet, Bertrand, Benoit Gabrielle, Claire Chenu, Dominique Arrouays, Jérôme Balesdent, Martial Bernoux, Elisa Bruni, Jean-Pierre Caliman, Rémi Cardinael, Songchao Chen, Philippe Ciais, Dominique Desbois, Julien Fouche, Stefan Frank, Catherine Henault, Emanuele Lugato, Victoria Naipal, Thomas Nesme, Michael Obersteiner, Sylvain Pellerin, David S. Powlson, Daniel P. Rasse, Frédéric Rees, Jean-François Soussana, Yang Su, Hanqin Tian, Hugo Valin, and Feng Zhou (2021) "Can N_2O emissions offset the benefits from soil organic carbon storage?" In: *Global Change Biology* 27.2, pp. 237–256. DOI: 10.1111/gcb.15342.

Højberg, Ole, Niels Peter Revsbech, and James M. Tiedje (1994) "Denitrification in Soil Aggregates Analyzed with Microsensors for Nitrous Oxide and Oxygen". In: *Soil Science Society of America Journal* 58.6, p. 1691. DOI: 10.2136/sssaj1994.03615995005800060016x.

John, Bettina, Tamon Yamashita, Bernard Ludwig, and Heiner Flessa (2005) "Storage of organic carbon in aggregate and density fractions of silty soils under different types of land use". In: *Geoderma* 128.1, pp. 63–79. DOI: 10.1016/j.geoderma.2004.12.013.

Keiluweit, Marco, Peter S. Nico, Markus Kleber, and Scott Fendorf (2016) "Are oxygen limitations under recognized regulators of organic carbon turnover in upland soils?" In: *Biogeochemistry* 127.2, pp. 157–171. DOI: 10.1007/s10533-015-0180-6.

Keiluweit, Marco, Tom Wanzek, Markus Kleber, Peter Nico, and Scott Fendorf (2017) "Anaerobic microsites have an unaccounted role in soil carbon stabilization". In: *Nature communications* 8.1, p. 1771. DOI: 10.1038/s41467-017-01406-6.

Kemmann, Björn, Lena Wöhl, Roland Fuß, Stefan Schrader, Reinhard Well, and Thorsten Ruf (2021) "N 2 and N 2 O mitigation potential of replacing maize with the perennial biomass crop Silphium perfoliatum —An incubation study". In: *GCB Bioenergy* 13.10, pp. 1649–1665. DOI: 10.1111/gcbb.12879.

Kölbl, Angelika, Jens Leifeld, and Ingrid Kögel-Knabner (2005) "A comparison of two methods for the isolation of free and occluded particulate organic matter". In: *Journal of Plant Nutrition and Soil Science* 168.5, pp. 660–667. DOI: 10.1002/jpln.200521805.

Kraus, Diana, Roland Brandl, Sebastian Achilles, Jörg Bendix, Paulina Grigusova, Annegret Larsen, Patricio Pliscoff, Kirstin Übernickel, and Nina Farwig (2022) "Vegetation and vertebrate abundance as drivers of bioturbation patterns along a climate gradient". In: *PloS one* 17.3, p. 0264408. DOI: 10.1371/journal.pone.0264408.

Kravchenko, Alexandra N. and Andrey K. Guber (2017) "Soil pores and their contributions to soil carbon processes". In: *Geoderma* 287, p. 3139. DOI: 10.1016/j.geoderma.2016.06.027.

Kravchenko, Alexandra N., Andrey K. Guber, Michelle Y. Quigley, John Koestel, Hasand Gandhi, and Nathaniel E. Ostrom (2018) "X-ray computed tomography to predict soil N 2 O production via bacterial denitrification and N 2 O emission in contrasting bioenergy cropping systems". In: *GCB Bioenergy* 10.11, pp. 894–909. DOI: 10.1111/gcbb.12552.

Kuzyakov, Yakov and Evgenia Blagodatskaya (2015) "Microbial hotspots and hot moments in soil: Concept & review". In: *Soil Biology and Biochemistry* 83, pp. 184–199. DOI: 10.1016/j.soilbio.2015.01.025.

Lacroix, Emily M., Meret Aeppli, Kristin Boye, Eoin Brodie, Scott Fendorf, Marco Keiluweit, Hannah R. Naughton, Vincent Noël, and Debjani Sihi (2023) "Consider the Anoxic Microsite: Acknowledging and Appreciating Spatiotemporal Redox Heterogeneity in Soils and Sediments". In: *ACS Earth and Space Chemistry*. DOI: 10.1021/acsearthspacechem.3c00032.

Lacroix, Emily M., Janica Mendillo, Anna Gomes, Anne Dekas, and Scott Fendorf (2022) "Contributions of anoxic microsites to soil carbon protection across soil textures". In: *Geoderma* 425, p. 116050. DOI: 10.1016/j.geoderma.2022.116050.

Legland, David, Ignacio Arganda-Carreras, and Philippe Andrey (2016) "MorphoLibJ: integrated library and plugins for mathematical morphology with ImageJ" in: *Bioinformatics (Oxford, England)* 32.22, p. 35323534. DOI: 10.1093/bioinformatics/btw413.

Leuther, Frederic, Robert Mikutta, Maximilian Wolff, Klaus Kaiser, and Steffen Schlüter (2023) "Structure turnover times of grassland soils under different moisture regimes". In: *Geoderma* 433, p. 116464. DOI: 10.1016/j.geoderma.2023.116464.

Leuthold, Sam J., Michelle L. Haddix, Jocelyn Lavallee, and M. Francesca Cotrufo (2023) "Physical fractionation techniques". In: *Encyclopedia of Soils in the Environment*. Elsevier, pp. 68–80. ISBN: 978-0-323-95133-3. DOI: 10.1016/B978-0-12-822974-3.00067-7.

Lewicka-Szczebak, Dominika, Jürgen Augustin, Anette Giesemann, and Reinhard Well (2017) "Quantifying N2O reduction to N2 based on N2O isotopocules – validation with independent methods (helium incubation and 15N gas flux method)". In: *Biogeosciences* 14.3, pp. 711–732. DOI: 10.5194/bg-14-711-2017.

Liang, Di and G. Philip Robertson (2021) "Nitrification is a minor source of nitrous oxide (N2 O) in an agricultural landscape and declines with increasing management intensity". In: *Global change biology* 27.21, pp. 5599–5613. DOI: 10.1111/gcb.15833.

Lucas, Maik, J. Gil, G. P. Robertson, N. E. Ostrom, and A. Kravchenko (2023) "Changes in soil pore structure generated by the root systems of maize, sorghum and switchgrass affect in situ N2O emissions and bacterial denitrification". In: *Biology and Fertility of Soils*. DOI: 10.1007/s00374-023-01761-1.

Lucas, Maik, Linh T. T. Nguyen, Andrey Guber, and Alexandra N. Kravchenko (2022) "Cover crop influence on pore size distribution and biopore dynamics: Enumerating root and soil faunal effects". In: *Frontiers in plant science* 13, p. 928569. DOI: 10.3389/fpls.2022.928569.

Lucas, Maik, James P. Santiago, Jinyi Chen, Andrey Guber, and Alexandra Kravchenko (2023) "The soil pore structure encountered by roots affects plant-derived carbon inputs and fate". In: *New Phytologist* 240.2, pp. 515–528. DOI: 10.1111/nph.19159.

Lucas, Maik, Steffen Schlüter, Hans-Jörg Vogel, and Doris Vetterlein (2019a) "Roots compact the surrounding soil depending on the structures they encounter". In: *Scientific reports* 9.1, p. 16236. DOI: 10.1038/s41598-019-52665-w.

— **(2019b)** "Soil structure formation along an agricultural chronosequence". In: *Geoderma* 350, pp. 61–72. DOI: 10.1016/j.geoderma.2019.04.041.

Lycus, Pawel, Manuel Jesús Soriano-Laguna, Morten Kjos, David John Richardson, Andrew James Gates, Daniel Aleksanteri Milligan, Åsa Frostegård, Linda Bergaust, and Lars Reier Bakken (2018) "A bet-hedging strategy for denitrifying bacteria curtails their release of N_2O" in: *Proceedings of the National Academy of Sciences* 115.46, pp. 11820–11825. DOI: 10.1073/pnas.1805000115.

Mendiburu, Felipe and Muhammad Yaseen (2020) *agricolae: Statistical Procedures for Agricultural Research*.

Morley, N. and E.M. Baggs (2010) "Carbon and oxygen controls on N2O and N2 production during nitrate reduction". In: *Soil Biology and Biochemistry* 42.10, pp. 1864–1871. DOI: 10.1016/j.soilbio.2010.07.008.

Ortega-Ramírez, Patricia, Valérie Pot, Patricia Laville, Steffen Schlüter, David Arturo Amor-Quiroz, Dalila Hadjar, Arnaud Mazurier, Marine Lacoste, Chloé Caurel, Valérie Pouteau, Claire Chenu, Isabelle Basile-Doelsch, Catherine Henault, and Patricia Garnier (2023) "Pore distances of particulate organic matter predict N2O emissions from intact soil at moist conditions". In: *Geoderma* 429, p. 116224. DOI: 10.1016/j.geoderma.2022.116224.

Ostrom, Peggy H., Samuel DeCamp, Hasand Gandhi, Joshua Haslun, and Nathaniel E. Ostrom (2021) "The influence of tillage and fertilizer on the flux and source of nitrous oxide with reference to atmospheric variation using laser spectroscopy". In: *Biogeochemistry*. DOI: 10.1007/s10533-020-00742-y.

Parkin, Timothy B. (1987) "Soil Microsites as a Source of Denitrification Variability". In: *Soil Science Society of America Journal* 51.5, pp. 1194–1199. DOI: 10.2136/sssaj1987.03615995005100050019x.

Philippot, Laurent, Sara Hallin, and Michael Schloter (2007) "Ecology of Denitrifying Prokaryotes in Agricultural Soil". In: Advances in Agronomy. Elsevier, pp. 249–305. ISBN: 978-0-12-374206-3. DOI: 10.1016/S0065-2113(07)96003-4.

Pires, Luiz F., Jaqueline A.R. Borges, Jadir A. Rosa, Miguel Cooper, Richard J. Heck, Sabrina Passoni, and Waldir L. Roque (2017) "Soil structure changes induced by tillage systems". In: *Soil and Tillage Research* 165, pp. 66–79. DOI: 10.1016/j.still.2016.07.010.

Qiu, Jianjun, Changsheng Li, Ligang Wang, Huajun Tang, Hu Li, and Eric Van Ranst (2009) "Modeling impacts of carbon sequestration on net greenhouse gas emissions from agricultural soils in China". In: *Global Biogeochemical Cycles* 23.1, 2008GB003180. DOI: 10.1029/2008GB003180.

R Core Team (2023) *R: A Language and Environment for Statistical Computing*. Vienna, Austria: R Foundation for Statistical Computing. URL: https://www.R-project.org/.

Rabot, E., M. Lacoste, C. Hénault, and I. Cousin (2015) "Using X-ray Computed Tomography to Describe the Dynamics of Nitrous Oxide Emissions during Soil Drying". In: *Vadose Zone Journal* 14.8, p. 2014120177. DOI: 10.2136/vzj2014.12.0177.

Ravishankara, A. R., John S. Daniel, and Robert W. Portmann (2009) "Nitrous oxide (N2O): the dominant ozone-depleting substance emitted in the 21st century". In: *Science (New York, N.Y.)* 326.5949, pp. 123–5. DOI: 10.1126/science.1176985.

Robertson, G. Philip (2023) "Denitrification and the challenge of scaling microsite knowledge to the globe". In: *mLife* 2.3, pp. 229–238. DOI: 10.1002/mlf2.12080.

Robertson, G.P. and P.M. Groffman (2024) "Nitrogen transformations". In: *Soil Microbiology, Ecology and Biochemistry*. Elsevier, pp. 407–438. ISBN: 978-0-12-822941-5. DOI: 10.1016/B978-0-12-822941-5.00014-4.

Rohe, Lena, Bernd Apelt, Hans-Jörg Vogel, Reinhard Well, Gi-Mick Wu, and Steffen Schlüter (2021) "Denitrification in soil as a function of oxygen availability at the microscale". In: *Biogeosciences* 18.3, pp. 1185–1201. DOI: 10.5194/bg-18-1185-2021.

Ruser, R., H. Flessa, R. Russow, G. Schmidt, F. Buegger, and J.C. Munch (2006) "Emission of N2O, N2 and CO2 from soil fertilized with nitrate: effect of compaction, soil moisture and rewetting". In: *Soil Biology and Biochemistry* 38.2, pp. 263–274. DOI: 10.1016/j.soilbio.2005.05.005.

Schindelin, Johannes, Ignacio Arganda-Carreras, Erwin Frise, Verena Kaynig, Mark Longair, Tobias Pietzsch, Stephan Preibisch, Curtis Rueden, Stephan Saalfeld, Benjamin Schmid, Jean-Yves Tinevez, Daniel James White, Volker Hartenstein, Kevin Eliceiri, Pavel Tomancak, and Albert Cardona (2012) "Fiji: an open-source platform for biological-image analysis". In: *Nature Methods* 9.7, pp. 676–682. DOI: 10.1038/nmeth.2019.

Schlüter, Steffen, Caroline Großmann, Julius Diel, Gi-Mick Wu, Sabine Tischer, Annette Deubel, and Jan Rücknagel (2018) "Long-term effects of conventional and reduced tillage on soil structure, soil ecological and soil hydraulic properties". In: *Geoderma* 332, p. 1019. DOI: 10.1016/j.geoderma.2018.07.001.

Schlüter, Steffen, Frederic Leuther, Lukas Albrecht, Carmen Hoeschen, Rüdiger Kilian, Ronny Surey, Robert Mikutta, Klaus Kaiser, Carsten W. Mueller, and Hans-Jörg Vogel (2022) "Microscale carbon distribution around pores and particulate organic matter varies with soil moisture regime". In: *Nature Communications* 13.1. DOI: 10.1038/s41467-022-29605-w.

Song, Xiaotong, Xiaotang Ju, Cairistiona F. E. Topp, and Robert M. Rees (2019) "Oxygen Regulates Nitrous Oxide Production Directly in Agricultural Soils". In: *Environmental Science & Technology* 53.21, pp. 12539–12547. DOI: 10.1021/acs.est.9b03089.

Stange, Florian C., Oliver Spott, Bernd Apelt, and Rolf W. B. Russow (2007) "Automated and rapid online determination of 15N abundance and concentration of ammonium, nitrite, or nitrate in aqueous samples by the SPINMAS technique". In: *Isotopes in Environmental and Health Studies* 43.3, pp. 227–236. DOI: 10.1080/10256010701550658.

Stolze, Katharina, Andrew D. Barnes, Nico Eisenhauer, and Kai U. Totsche (2022) "Depth-differentiated, multivariate control of biopore number under different land-use practices". In: *Geoderma* 418, p. 115852. DOI: 10.1016/j.geoderma.2022.115852.

Surey, Ronny, Corinna M. Schimpf, Leopold Sauheitl, Carsten W. Mueller, Pauline S. Rummel, Klaus Dittert, Klaus Kaiser, Jürgen Böttcher, and Robert Mikutta (2020) "Potential denitrification stimulated by water-soluble organic carbon from plant residues during initial decomposition". In: *Soil Biology and Biochemistry* 147, p. 107841. DOI: 10.1016/j.soilbio.2020.107841.

Tian, Hanqin, Rongting Xu, Josep G. Canadell, Rona L. Thompson, Wilfried Winiwarter, Parvadha Suntharalingam, Eric A. Davidson, Philippe Ciais, Robert B. Jackson, Greet Janssens-Maenhout, Michael J. Prather, Pierre Regnier, Naiqing Pan, Shufen Pan, Glen P. Peters, Hao Shi, Francesco N. Tubiello, Sönke Zaehle, Feng Zhou, Almut Arneth, Gianna Battaglia, Sarah Berthet, Laurent Bopp, Alexander F. Bouwman, Erik T. Buitenhuis, Jinfeng Chang, Martyn P. Chipperfield, Shree R. S. Dangal, Edward Dlugokencky, James W. Elkins, Bradley D. Eyre, Bojie Fu, Bradley Hall, Akihiko Ito, Fortunat Joos, Paul B. Krummel, Angela Landolfi, Goulven G. Laruelle, Ronny Lauerwald, Wei Li, Sebastian Lienert, Taylor Maavara, Michael MacLeod, Dylan B. Millet, Stefan Olin, Prabir K. Patra, Ronald G. Prinn, Peter A. Raymond, Daniel J. Ruiz, Guido R. van der Werf, Nicolas Vuichard,

Junjie Wang, Ray F. Weiss, Kelley C. Wells, Chris Wilson, Jia Yang, and Yuanzhi Yao (2020) "A comprehensive quantification of global nitrous oxide sources and sinks". In: *Nature* 586.7828, pp. 248–256. DOI: 10.1038/s41586-020-2780-0.

Wagai, Rota, Lawrence M. Mayer, and Kanehiro Kitayama (2009) "Nature of the "occluded" low-density fraction in soil organic matter studies: A critical review". In: *Soil Science and Plant Nutrition* 55.1, pp. 13–25. DOI: 10.1111/j.1747-0765.2008.00356.x.

Wardak, D. Luke R., Faheem N. Padia, Martine I. De Heer, Craig J. Sturrock, and Sacha J. Mooney (2022) "Zero tillage has important consequences for soil pore architecture and hydraulic transport: A review". In: *Geoderma* 422, p. 115927. DOI: 10.1016/j.geoderma.2022.115927.

Wei, Huanhuan, Xiaotong Song, Yan Liu, Rui Wang, Xunhua Zheng, Klaus Butterbach-Bahl, Rodney T. Venterea, Di Wu, and Xiaotang Ju (2023) "In situ 15N-N2O site preference and O2 concentration dynamics disclose the complexity of N2O production processes in agricultural soil". In: *Global Change Biology* 29.17, pp. 4910–4923. DOI: 10.1111/gcb.16753.

Weier, K. L., J. W. Doran, J. F. Power, and D. T. Walters (1993) "Denitrification and the Dinitrogen/Nitrous Oxide Ratio as Affected by Soil Water, Available Carbon, and Nitrate". In: *Soil Science Society of America Journal* 57.1, pp. 66–72. DOI: 10.2136/sssaj1993.03615995005700010013x. URL: http://doi.wiley.com/10.2136/sssaj1993.03615995005700010013x (visited on 03/16/2024)

White, Rosemary G. and John A. Kirkegaard (2010) "The distribution and abundance of wheat roots in a dense, structured subsoil–implications for water uptake". In: *Plant, cell & environment* 33.2, pp. 133–48. DOI: 10.1111/j.1365-3040.2009.02059.x.

Wilkinson, Marshall T., Paul J. Richards, and Geoff S. Humphreys (2009) "Breaking ground: Pedological, geological, and ecological implications of soil bioturbation". In: *Earth-Science Reviews* 97.1, pp. 257–272. DOI: 10.1016/j.earscirev.2009.09.005.

Yang, Xue-Ming and Michelle M. Wander (1999) "Tillage effects on soil organic carbon distribution and storage in a silt loam soil in Illinois". In: *Soil and Tillage Research* 52.1, p. 19. DOI: 10.1016/S0167-1987(99)00051-3.

You, Yongfa, Hanqin Tian, Shufen Pan, Hao Shi, Chaoqun Lu, William D. Batchelor, Bo Cheng, Dafeng Hui, David Kicklighter, Xin-Zhong Liang, Xiaoyong Li, Jerry Melillo, Naiqing Pan, Stephen A. Prior, and John Reilly (2024) "Net greenhouse gas balance in U.S. croplands: How can soils be part of the climate solution?" In: *Global Change Biology* 30.1, e17109. DOI: 10.1111/gcb.17109.

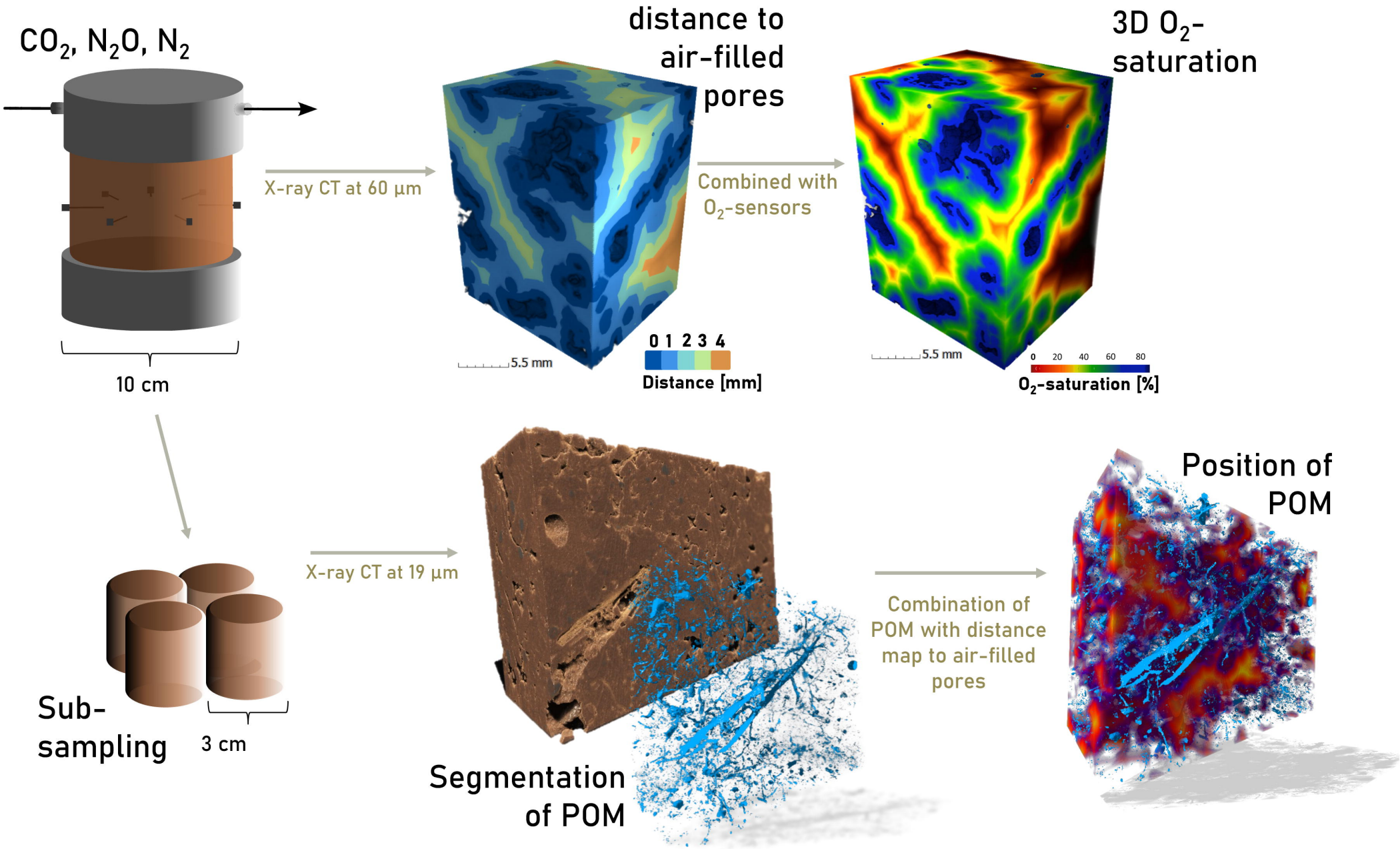
CO_2, N_2O, N_2
10 cm
X-ray CT at 60 µm
distance to air-filled pores
5.5 mm
0 1 2 3 4
Distance [mm]
Combined with O_2-sensors
3D O_2-saturation
5.5 mm
0 20 40 60 80
O_2-saturation [%]
Sub-sampling
3 cm
X-ray CT at 19 µm
Segmentation of POM
Combination of POM with distance map to air-filled pores
Position of POM

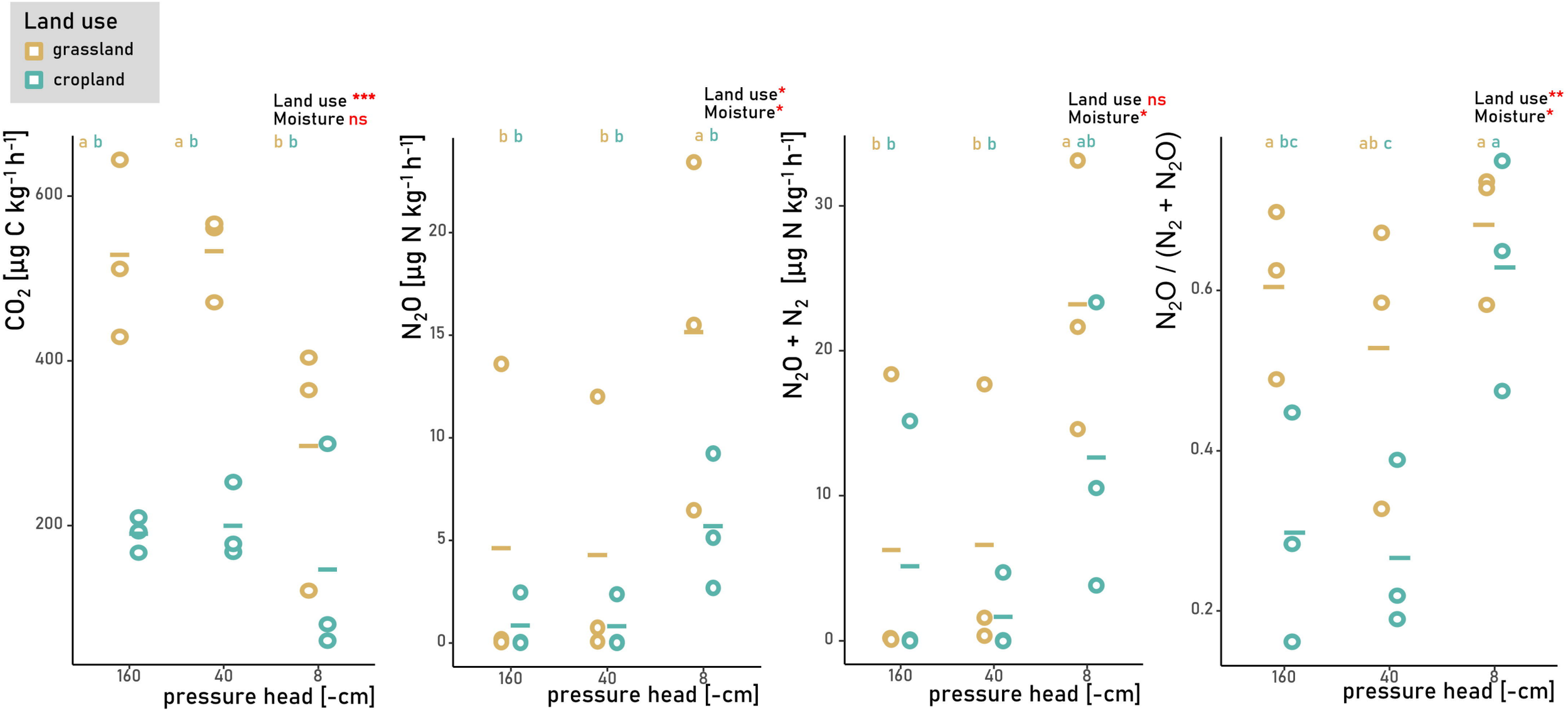
Land use
grassland
cropland
Land use ***
Moisture ns
a b
a b
b b
CO2 [µg C kg-1 h-1]
600
400
200
160
40
8
pressure head [-cm]
Land use*
Moisture*
b b
b b
a b
N2O [µg N kg-1 h-1]
20
15
10
5
0
160
40
8
pressure head [-cm]
Land use ns
Moisture*
b b
b b
a ab
N2O + N2 [µg N kg-1 h-1]
30
20
10
0
160
40
8
pressure head [-cm]
Land use**
Moisture*
a bc
ab c
a a
N2O / (N2 + N2O)
0.6
0.4
0.2
160
40
8
pressure head [-cm]

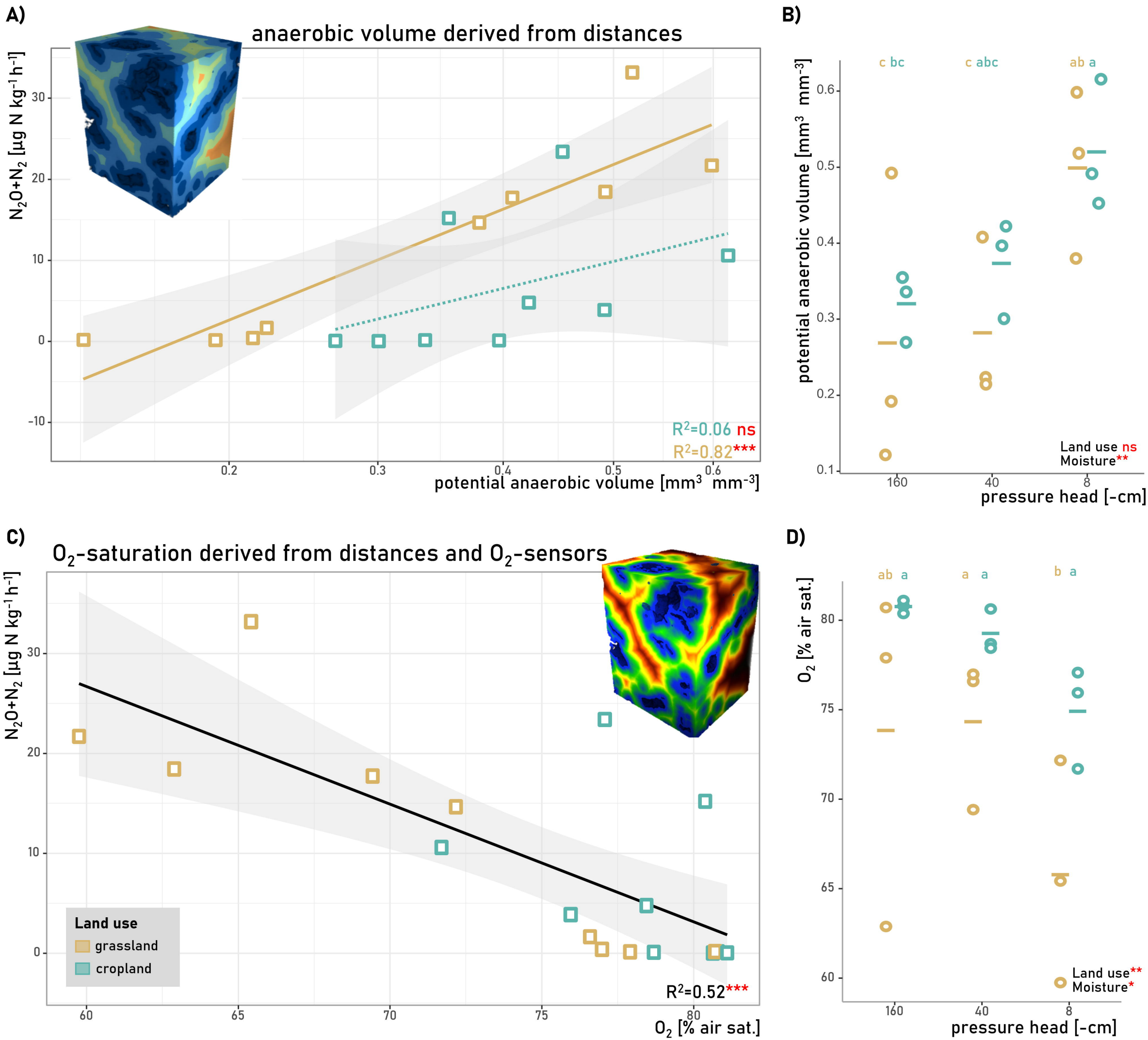
A)
anaerobic volume derived from distances
N2O+N2 [µg N kg-1 h-1]
potential anaerobic volume [mm3 mm-3]
R2=0.06 ns
R2=0.82***
B)
c bc
c abc
ab a
potential anaerobic volume [mm3 mm-3]
Land use ns
Moisture**
pressure head [-cm]
C)
O2-saturation derived from distances and O2-sensors
N2O+N2 [µg N kg-1 h-1]
Land use
grassland
cropland
R2=0.52***
O2 [% air sat.]
D)
ab a
a a
b a
O2 [% air sat.]
Land use**
Moisture*
pressure head [-cm]

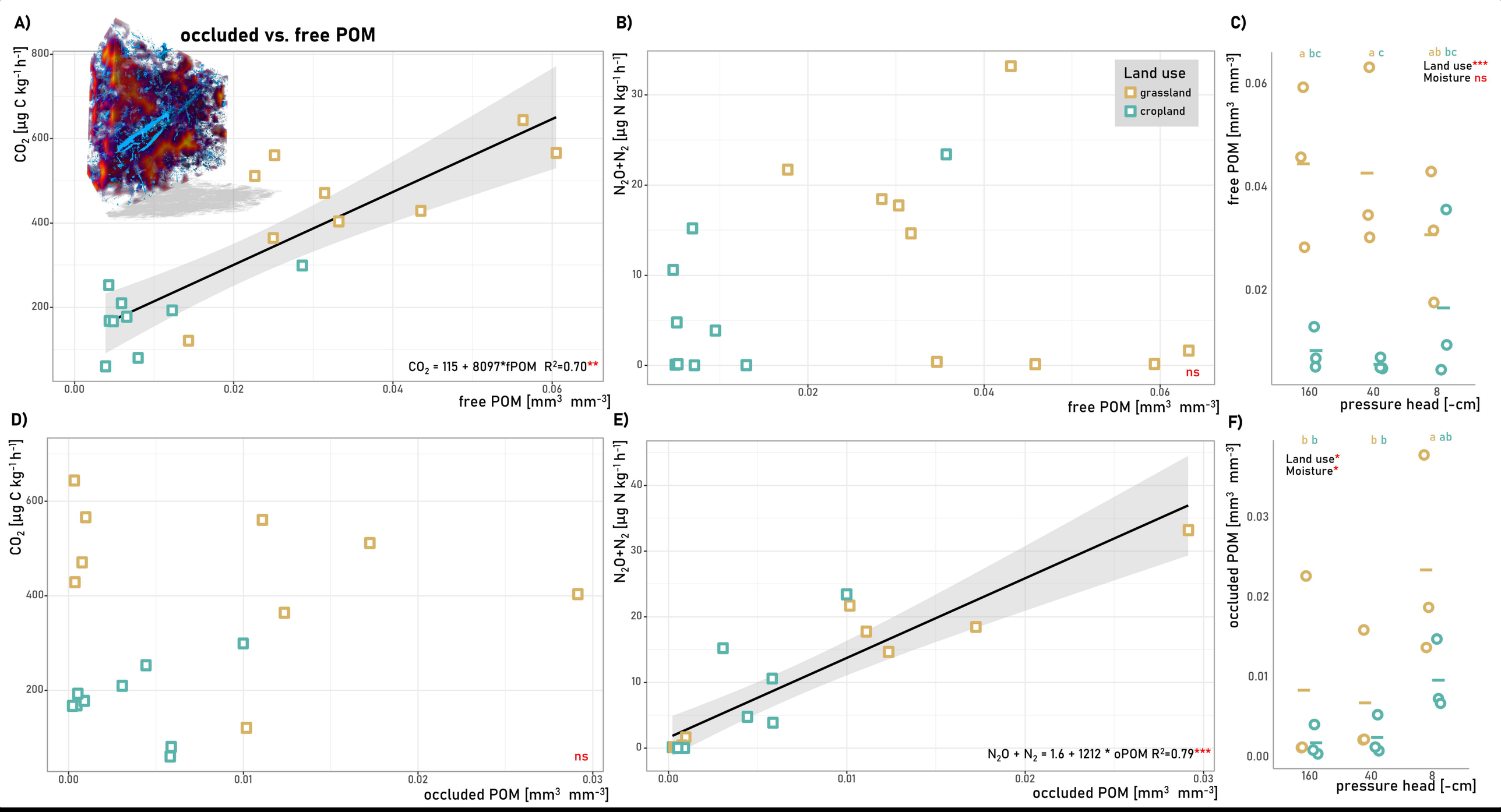
A)
occluded vs. free POM
CO2 [µg C kg-1 h-1]
CO2 = 115 + 8097*fPOM R2=0.70**
free POM [mm3 mm-3]
B)
N2O+N2 [µg N kg-1 h-1]
Land use
grassland
cropland
ns
free POM [mm3 mm-3]
C)
free POM [mm3 mm-3]
a bc
a c
ab bc
Land use***
Moisture ns
pressure head [-cm]
D)
CO2 [µg C kg-1 h-1]
ns
occluded POM [mm3 mm-3]
E)
N2O+N2 [µg N kg-1 h-1]
N2O + N2 = 1.6 + 1212 * oPOM R2=0.79***
occluded POM [mm3 mm-3]
F)
occluded POM [mm3 mm-3]
b b
b b
a ab
Land use*
Moisture*
pressure head [-cm]

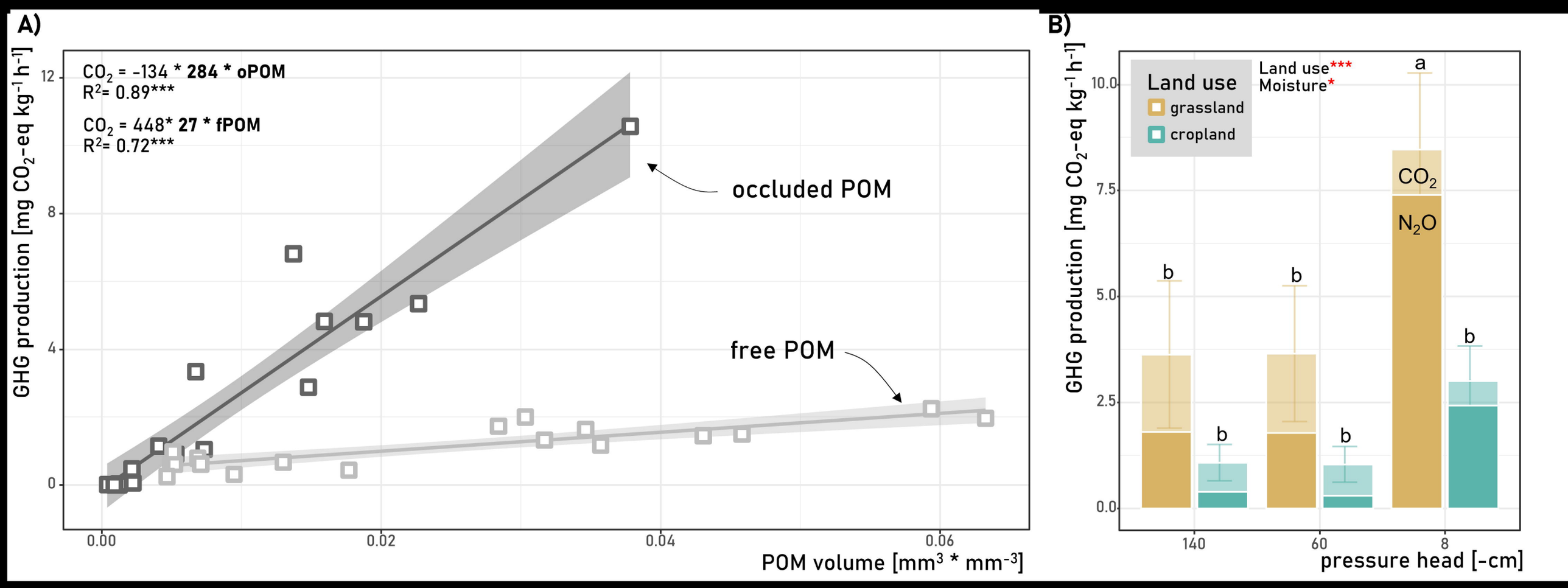
A)
CO_2 = -134 * 284 * oPOM
R^2= 0.89***
CO_2 = 448* 27 * fPOM
R^2= 0.72***
occluded POM
free POM
GHG production [mg CO_2-eq kg^{-1} h^{-1}]
POM volume [mm^3 * mm^{-3}]
0.00
0.02
0.04
0.06
0
4
8
12
B)
Land use
grassland
cropland
Land use***
Moisture*
CO_2
N_2O
a
b
b
b
b
b
GHG production [mg CO_2-eq kg^{-1} h^{-1}]
pressure head [-cm]
140
60
8
0.0
2.5
5.0
7.5
10.0

Grassland with free POM and occluded POM

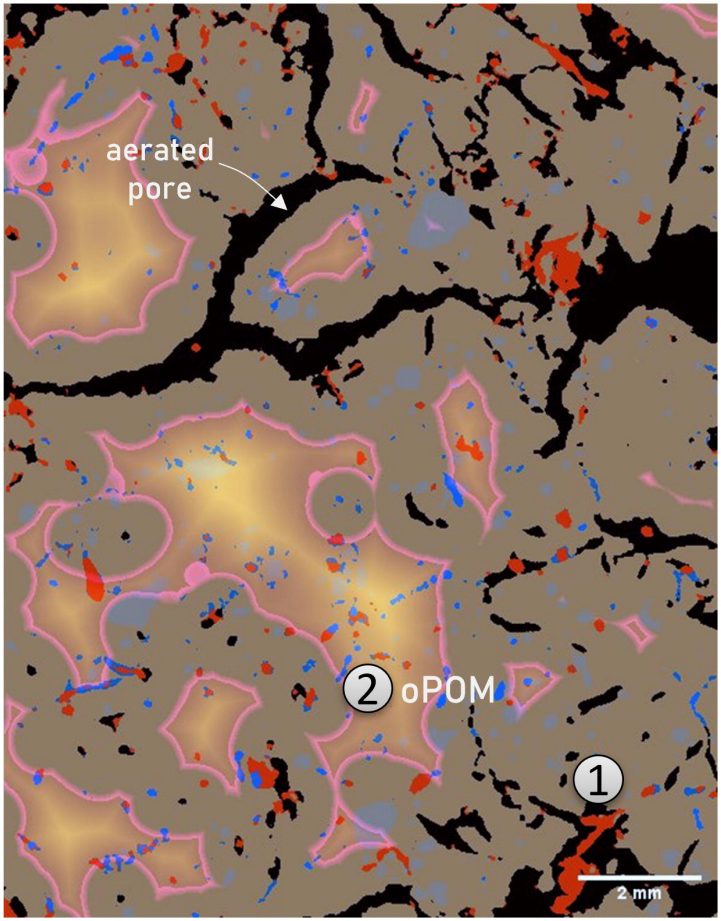

Cropland with predominately free POM

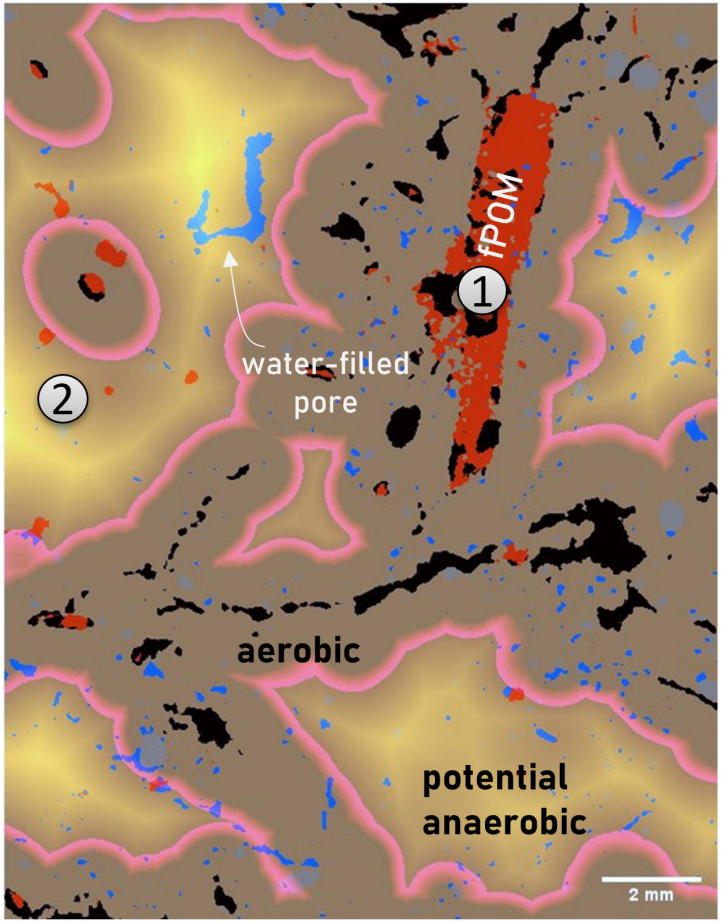

① Hotspot for respiration ② Hotspot for denitrification